SELECTIVE PLASMONIC CONTROL OF EXCITONS AND THEIR NON-RADIATIVE ENERGY TRANSFER IN COLLOIDAL SEMICONDUCTOR QUANTUM DOT SOLIDS

A THESIS
SUBMITTED TO THE DEPARTMENT OF PHYSICS
AND THE INSTITUTE OF ENGINEERING AND SCIENCES
OF BILKENT UNIVERSITY
IN PARTIAL FULLFILMENT OF THE REQUIREMENTS
FOR THE DEGREE OF
MASTER OF SCIENCE

By
Tuncay Özel
August 2009

I certify that I have read this thesis and that in my opinion it is fully adequate, in scope and in quality, as a thesis for the degree of Master of Science.

Assist. Prof. Dr. Hilmi Volkan Demir (Supervisor)

I certify that I have read this thesis and that in my opinion it is fully adequate, in scope and in quality, as a thesis for the degree of Master of Science.

Assist. Prof. Dr. Dönüş Tuncel

I certify that I have read this thesis and that in my opinion it is fully adequate, in scope and in quality, as a thesis for the degree of Master of Science.

Assist. Prof. Dr. Coşkun Kocabaş

Approved for the Institute of Engineering and Sciences:

Prof. Dr. Mehmet B. Baray
Director of Institute of Engineering and Sciences

ABSTRACT

SELECTIVE PLASMONIC CONTROL OF EXCITONS AND THEIR NON-RADIATIVE ENERGY TRANSFER IN COLLOIDAL SEMICONDUCTOR QUANTUM DOT SOLIDS

Tuncay Özel

M.S. in Physics

Supervisor: Assist. Prof. Dr. Hilmi Volkan Demir

August 2009

To date extensive research has proved that semiconductors and metals exhibit extraordinary optical properties in nano-dimensions compared to their bulk counterparts. For example, an interesting effect is observed in metal nanostructures/nanoparticles (NPs) that we form to obtain localized plasmons, with their optical response highly tuneable using the size effect. Another field of interest at the nanoscale is the investigation of light generation and harvesting using colloidal semiconductor quantum dot nanocrystals (NCs) that we synthesize in few nanometers, with their emission and absorption excitonic peaks conveniently tuneable using the size effect. In this thesis, we proposed and demonstrated the first accounts of selectively plasmonically-controlled colloidal quantum dot emitters assembled in innovative architectures, with a control achieved either through spatial selection or spectral selection. In the first set of designs, we developed for the first time plasmonic NC-composites that rely on spatially-selected plasmon-coupled CdTe NC-monolayers interspaced with respect to Au NP-monolayers in a repeating three-dimensional layer-by-layer architecture. In these bottom-up designs of hybrid nanocomposites, the photoluminescence kinetics is strongly modified and a record quantum efficiency of 30% is achieved for such CdTe NC solids. In the second set of

designs, we showed the first spectrally-selected plasmon-coupling of surface-emitting CdS NCs using optimized Ag NP deposits. This architecture allowed for the surface-state emission to be selectively enhanced while the interband emission is simultaneously suppressed in the same plasmon-coupled NCs, leading to the strongest surface-state emission from such CdS NCs reported with respect to their interband emission (with a >12-fold enhancement). Yet another important proximity phenomenon effective among quantum dot emitters is the Förster-type non-radiative resonance energy transfer (ET), in which excitonic excitation energy of the donor-NCs is non-radiatively transferred to the acceptor-NCs via dipole-dipole coupling. In the third set of our designs, we combined two fundamental proximity mechanisms of plasmon coupling and non-radiative energy transfer in the same NC solids. In plasmonic ET, we reported for the first time selectively plasmon-coupling of NC-acceptors and then that of NC-donors in the ET pair, both of which result in substantial enhancement of the acceptor emission with respect to ET with no plasmon coupling (with a maximum of 2-fold enhancement) as verified by their steady-state and time-resolved photoluminescence. This concept of spectrally/spatially-selective plasmon coupling in quantum dots paves a new path for devices and sensors in nanophotonics.

Keywords: Plasmonics, localized plasmons, metal nanoparticles, metal nanostructures; non-radiative Förster energy transfer; semiconductor nanocrystals, colloidal quantum dots; excitons, spontaneous emission, photoluminescence, metal-enhanced luminescence; FDTD.

ÖZET

KOLLOİDAL YARIİLETKEN KUVANTUM NOKTACIK FİLMLERİNDE EKZİTONLARIN SEÇİMLİ PLAZMONİK KONTROLÜ VE RADYASYONSUZ ENERJİ TRANSFERLERİ

Tuncay Özel
Fizik Bölümü Yüksek Lisans
Tez Yöneticisi: Yrd. Doç. Dr. Hilmi Volkan Demir
Ağustos 2009

Bugüne kadar yapılan kapsamlı araştırmalar sonucu yarıiletken ve metallerin nano parçacık boyutlarına küçültüldüğünde normal boyutlarında göstermedikleri olağan dışı optik özellikler gösterdikleri ispatlanmıştır. Mesela, metal nanoparçacık/nanoyapılarda (NPs) görülen bir özellik, boyut etkisi ile optik özelliklerin değişimi ve bu sayede elde edilen lokalize plazmonlardır. Nanometrik boyutlarda başka bir ilgi alanı ise birkaç nanometre boyutlarında sentezlenen kuvantum sınırlandırma boyut etkisi ile ışıma ve emilim ekzitonik tepe noktalarının değiştirilebilirliği olan yarıiletken kuvantum noktacık nanokristallerin (NCs) ışık üretimi ve ışık emilimi için kullanımıdır. Bu tezde, kolloidal kuvantum noktacık ışıyanlarının seçimli plazmonik kontrollerini yenilikçi mimariler ile pozisyonsal ve spektrumsal seçimlerle yapılabileceğini öne sürüyor ve öncü çalışmalarını gerçekleştiriyoruz. İlk dizaynda, Au nanoparçacık tek katmanlarının, pozisyonsal seçimli plazmon resonans etkisi ile CdTe nanokristal tek katmanları katman katman tekrar eden üç boyutlu bir mimaride plazmonik NC-kompozitleri ilk defa gösterilmiştir. Dizaynı aşağıdan yukarıya olan bu hibrit nanokompozitlerin fotoışıma özellikleri ciddi bir şekilde değişime uğramıştır ve CdTe nanokristal filmlerinde %30 ile rekor bir kuvantum verimliliği elde edilmiştir. İkinci dizaynda, yüzeyden ışıyan CdS

nanokristallerinin Ag nanoadacık üretimi ile spektral seçimli plazmonik etkileşimi sağlanmıştır. Bu mimari ile plazmon ile eşleşen aynı nanokristalin yüzey enerji seviyelerinde üretilen ışıma arttırılmış olup eş zamanlı ana bant enerji seviyesindeki ışımasının azaltılması ile CdS nanokristallerde en yüksek yüzey ışıma/bant ışıma oranı (12 kat artış ile) elde edilmiştir. Kuvantum noktacıklarının yakınlarında oluşan bir başka etki ise ekzitonik uyarma enerjisinin verici (donor) nanokristalden alıcı (acceptor) nanokristale dipol-dipol etkileşimi ile radyasyonsuz bir şekilde aktarıldığı Förster tipi enerji transferidir (ET). Üçüncü dizaynda, iki ana etkileşim olan plazmon etkileşimi ve radyasyonsuz enerji transferi etkileşimini aynı nanokristal film için birleştirdik. Plazmonik ET ile ilk defa verici ve alıcı nanokristale seçimli plazmonik etkileşim uygulanarak alıcı nanokristalin ışıması iki örnekte de önemli bir oranda (maksimum 2 kat) arttırıldığı sabit ve zaman çözünürlü fotoışıma ölçümleri ile gösterilmiştir. Nanokristalleri spektral ve pozisyonsal olarak birleştirme konsepti, nanofotonik aygıt ve sensör yapımında yeni bir yol olmaktadır.

Anahtar sözcükler: Plazmonik, lokalize plazmonlar, metal nanoparçacıklar, metal nanoyapılar, radyasyonsuz Förster enerji transferi, yarıiletken nanokristaller, kolloidal quantum noktacıklar, ekzitonlar, kendiliğinden ışınsalım, fotoışıma, metalle artırılan ışıma, zamanda sonlu farklar; FDTD.

Acknowledgements

I would like to thank my supervisor Asst. Prof. Dr. Hilmi Volkan Demir for his endless support from the beginning of my academic career. He always wanted the best for me and encouraged me to do so. His positive attitude to life has been always a trigger and motivation for me.

I would like to thank Asst. Prof. Dr. Dönüş Tuncel for her guidance and support in our collaborative research works and also giving useful comments and suggestions as being a member of my thesis committee.

I would like to thank Asst. Prof. Dr. Coşkun Kocabaş for his contributions and guidance during my research efforts and also giving useful comments and suggestions as being a member of my thesis committee.

I would like to thank my brother Taner Özel for his answers to my endless questions, and being a good model for me as a physicist and as a person.

I would like to thank all former and recent group members of Devices and Sensors Group, who work under the supervision of H. Volkan Demir. I would especially like to thank Olga Samarskaya, Murat Soğancı, Nihan Kosku Perkgöz, Aslı Yılmaz, Neslihan Çiçek, Gülis Zengin, Emre Sarı, Can Uran, Gürkan Polat, Akın Sefünç, Özgun Akyüz, Emre Ünal, Sina Toru, Talha Erdem, Burak Güzeltürk, Uğur Karatay, and Hatice Ertuğrul for their friendship and collaborations.

There are especially some very special friends to me whom I feel like my family members. These are Evren Mutlugün who is a cheer supply for me all the time, Rohat Melik who always treated me like his younger brother, Sedat Nizamoğlu who is always kind and very helpful in my research, Özgür Çakmak who is the

most generous person I have ever seen. Those are very special friends to me and they were always there when I needed them.

I would like to thank the team “2+1”. Part of that team is me, Seçkin Şenlik and Samed Yumrukçu (as +1). I am glad to be sharing such a nice friendship, which we hope will never end. I always feel very lucky to be their close friends. I hope life treats them very well in the future and this friendship goes forever.
I want to say how glad I am to meet those very special ladies whom made my friends very happy; Özlem Şenlik, Şeyda İpek, Sümeyye Mutlugün, and Bahar Melik.

I would also like to thank my family Ali and Yıldız Özel for their endless love and support which helped me a lot to achieve my goals since my childhood.
I would like to thank to my new family members, İlhan, Ayhan, Ulaş, and Simge Huyal for being always kind to me and sharing their “little precious” with me.

Finally, I would like to thank to my beautiful wife for our past, present, future and everything…I am very grateful to her love and trust on me. She was also very helpful during my undergraduate and graduate studies and made fruitful contributions to my research efforts. Additionally I want to thank for her support and patience during preparation of my thesis defense. I want to share our great love with you forever.

Table of Contents

List of Figures

List of Tables

To my wife…

Chapter 1

Introduction

In the last few decades nanotechnology in scientific research has gained increasingly more attention via the recent technological developments achieved in science and engineering. New fabrication and characterization tools enabled scientists to extend their research into smaller structures and particles in nano-dimensions. As a result, to date extensive research has showed that semiconductors and metals exhibit extraordinary optical properties in nano-dimensions compared to their bulk forms.

One of the most attractive fields of interest at nanoscale is plasmonics because of its wide range of possible applications in photonics. The use of plasmons dates back to the 4th century (A.D.) with the famous Lycurgus cup, which is made for decorative purposes to change its color when there is a light source put inside the cup [1]. It took many centuries to understand the underlying physical mechanism that leads to this change of the color in the cup. At the 19th century Michael Faraday was the first one who could enlighten this mystery of the Lycurgus cup [2]. Only in the beginning of the 20th century Mie solved the Maxwell equations for spherical particles to present their extinction properties at different sizes of the spheres [3]. Even though these scientific contributions were made to literature about a century ago, it took so long for scientists to

discuss and develop the surface plasmon theory and demonstrate experiments to verify and utilize this theory. Now with the recent developments in nanotechnology, there have been a great interest and progress in the investigation of photo-physical properties of surface plasmons as well as in their use for many different photonic applications including metal-enhanced fluoresce [4], surface-enhanced Raman spectroscopy [5], plasmon-enhanced nonlinear optical processes [6], and plasmon-mediated two-photon absorption [7].

Another attractive field of interest at the nano scale is the investigation of light generating and harvesting using semiconductor colloidal nanocrystals (NCs) for their potential use in different applications such as solid-state lighting [8], photovoltaics [9], and bio-labeling [10]. Colloidal nanocrystals can be synthesized in a few nanometers and their emission/absorption wavelengths can be conveniently tuned by the change of their size during the synthesis. This is called the size effect, which provides a significant flexibility for the optical applications of nanocrystals (since a targeted emission/absorption wavelength can be achieved especially in the visible and near-IR spectra). Also using different kind of combinations of metals it is possible to tune the emission wavelength of NCs in wide spectral ranges. Nanocrystals can also be easily embedded into a variety of structures in hybrid architectures (e.g., in polymers) because they can be prepared in different kinds of solvents and their surface can be positively or negatively charged by modification of their ligands.

The use of nanocrystals in light generation and harvesting applications necessitates the demonstration of highly efficient NC emitters. However, the quantum efficiency of colloidal NCs unfortunately decreases with the film formation [11]. To address this problem, metal-enhanced fluorescence methodology can be used by plasmon coupling of these NC film layers to achieve a substantial increase in the resulting film quantum efficiency. This is possible through the plasmon resonance energy transfer between NCs and metal nanoparticles (NPs) that alters emission characteristics of excited NCs via

enhanced localized electric field created by plasmonic oscillations [12]. Since the emission properties of nanocrystals can be modified by the surface plasmons generated in metal nanoparticles (NPs), it is expected to observe significant changes in radiative and decay rates of NC photoluminescence. One favored result of this mechanism is the spontaneous emission enhancement of quantum dots in the close vicinity of metal NPs [13,14]. Nanocrystal emission can be enhanced (quenched) via plasmonic coupling as a result of the increase in the radiative (non-radiative) decay rates under certain conditions. Separation between metal nanoparticles and nanocrystals, spectral match between plasmon resonance wavelength of metal nanoparticles and emission wavelength of nanocrystals are important conditions effecting nanocrystal emission mechanisms [15,16]. In our NC film layers we optimize all of the spectral and thickness conditions to observe the highest quantum efficiencies using surface plasmons.

Förster resonance energy transfer (FRET) is an important proximity phenomenon, also effective among NCs. In FRET excitation energy of donor nanocrystals is non-radiatively transferred to acceptor nanocrystals by coupling of the donor nanocrystal emission to the excitation of the acceptor nanocrystal [12,17]. The possibility to modify energy transfer between donor and acceptor NCs is of fundamental importance for the physical aspects of NC embedded photonic devices. Here we combine two fundamental energy transfer mechanisms FRET and plasmon resonance energy transfer between NC and metal NP and present plasmonic coupling of FRET between two differently sized (donor-acceptor) CdTe quantum dot nanocrystals using metal nanoparticles. We report on the steady-state and time-resolved photoluminescence properties of these plasmon coupled NCs interacting with each other via FRET and analyze consequent modifications of their emission kinetics through plasmon-coupled FRET. We investigate the FRET mechanism under the plasmon coupling to only donor NCs and only acceptor NCs.

Our research interest mainly focuses on the understanding and the development of highly efficient emitters/absorbers using energy transfer mechanisms. We are especially interested in two main energy transfer mechanisms, resonance energy transfer between metal nanoparticles and nanocrystals, and Förster resonance energy transfer between two differently sized nanocrystals.

In Chapter 1, we present a brief introduction on nanostructures and energy transfer mechanisms. The importance and the use of nanocrystals and metal nanoparticles in nanotechnology are explained with some examples. Here we also briefly discuss our solutions to the problems investigated in this thesis.

In Chapter 2, we provide a background on the fundamentals of surface plasmons. We introduce localized plasmons and surface plasmon resonance of the metal nanoparticles. Size, shape, composition, and environment dependency of surface plasmon resonance is discussed.

In Chapter 3, we summarize the theoretical aspects of nanocrystals with their applications in the literature. We also present the CdTe NC synthesis along with their optical characterization results.

In Chapter 4, we show plasmonic coupling of nanocrystals in a three-dimensional construction by repeating unit cells of semiconductor NC and metal nanoparticle layers. We present our results showing a significant emission enhancement of NC layers while their fluorescence decay lifetimes are shortened by repeating our unit cell architecture.

In Chapter 5, we begin with providing some background on the surface-state emitting (SSE) CdS NCs and their importance in white light generation. We present our results, which show a significant enhancement in surface state emission compared to the band-edge emission by plasmonic coupling to trap states of SSE CdS NCs.

In Chapter 6, we combine two fundamental energy transfer mechanisms and present plasmonic coupling of FRET between two differently sized (donor-acceptor) CdTe quantum dot nanocrystals using metal nanoparticles. We report on steady-state and time-resolved photoluminescence properties of these plasmon-coupled NCs interacting with each other via FRET and analyze consequent modifications of their emission kinetics through plasmon-coupled FRET.

Chapter 2

Fundamentals of Surface Plasmons

Collective oscillations of negatively charged electrons arising at the interface between a dielectric and a conductor are called surface plasmons [18]. Surface plasmons can appear in different forms including freely propagating electromagnetic surface waves along metal surfaces and localized electron oscillations confined in metal nanoparticles. Resulting electromagnetic fields are quite different from each other, which can be deduced by the modified boundary conditions of corresponding solutions to Maxwell equations. We will investigate surface plasmons through localized surface plasmons which is generated in metal nanoparticles and mostly used for emission enhancement and surface-enhanced Raman spectroscopy applications.

2.1 Surface Plasmon Resonance

In the presence of incident electromagnetic radiation, metal nanoparticles (NPs) show different optical responses compared to flat metal surfaces. In 1908, Mie made a great contribution to literature by solving the Maxwell equations for spherical particles, which enlightened the scattering and absorption characteristics of spherical particles in various sizes [3]. However particles with very small dimensions need more careful treatment due to formation of surface plasmons.

The characteristic optical response of metal NPs comes from the presence of surface plasmon resonance generated by collective oscillations of conduction electrons and the incident electromagnetic wave. Surface plasmons create a strong electric field around the nanoparticle that vanishes away exponentially by distance [19]. Surface plasmon resonance is well observed as the particle size decreases especially to the sizes in the range of penetration depth into metal. This is because external electromagnetic field (incident radiation) can penetrate into the whole particle and results in a significant shift in the positions of free electrons on the metal surface. The penetration depth is on the order of 30 nm for Ag and Au metals, which necessitates the formation metal particles smaller than size [20]. This is the main reason that localized surface plasmon research can be only conducted by the use of nanoscale metal particles (nanoparticles). In such metal nanoparticles surface plasmon resonance are formed as the electromagnetic field waves of the incident radiation penetrate into the metal NP and shift the conduction electrons from the nucleus. This generates a polarization on the particle (with a sinusoidally varying electric field) and then a restoring force is generated due to the Coulomb attraction force between the fixed positive ions at the nucleus and the conduction electrons as depicted in Fig. 2.1 [21]. This restoring force is produced as the electrons move back and forth and creates the oscillation. The frequency of this oscillation is called the surface plasmon resonance frequency.

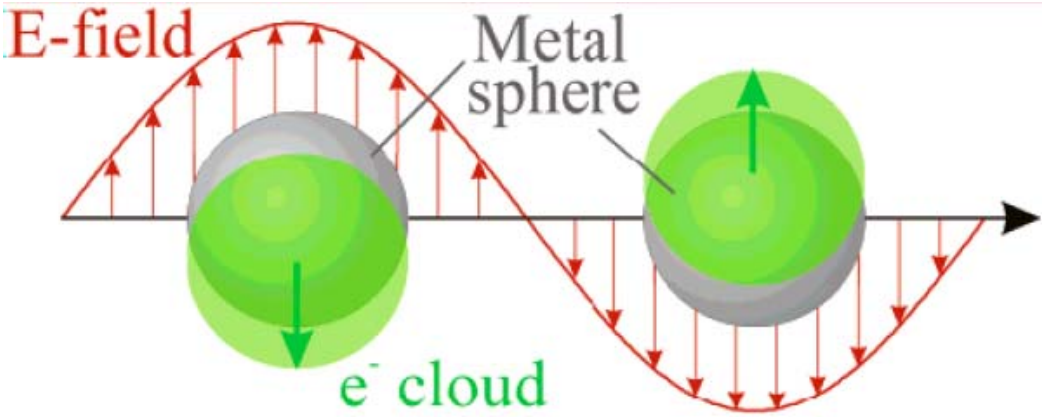

Figure 2.1. Schematic representation of electric field due to an incident wave and corresponding shift of electron cloud resulting in a plasmon resonance of the particle [21].

Surface plasmon resonance frequency directly depends on the material type. For instance Al, Pb, and Hg metals have very high frequencies corresponding to UV wavelength region. On the other case Au and Ag nanoparticles have resonance wavelengths corresponding to the visible region. For this reason these metal are widely used in emission enhancement experiments of visible emitters.

Classical surface plasmon resonance is given in (1)

$$\omega = \left(\frac{e^2}{\varepsilon_0 m_e 4\pi\, r_s^3}\right)^{1/2} \tag{1}$$

where ε_0 is the vacuum permittivity, m_e is the effective mass, and r_s is radius of the sphere. As can be seen from the equation, nanoparticle size is inversely proportional to the resonance frequency [22].

We make FDTD calculations using a commercially available program by Lumerical Solutions Inc. (Vancouver, Canada) to observe the effect of incident radiation on the near-field enhancement around the metal nanoparticles. We observe that the electric field intensity is maximized on the surface of nanoparticles at the direction of polarization of the incident radiation and decays at very small distances as depicted in Fig. 2.2 and Fig. 2.3.

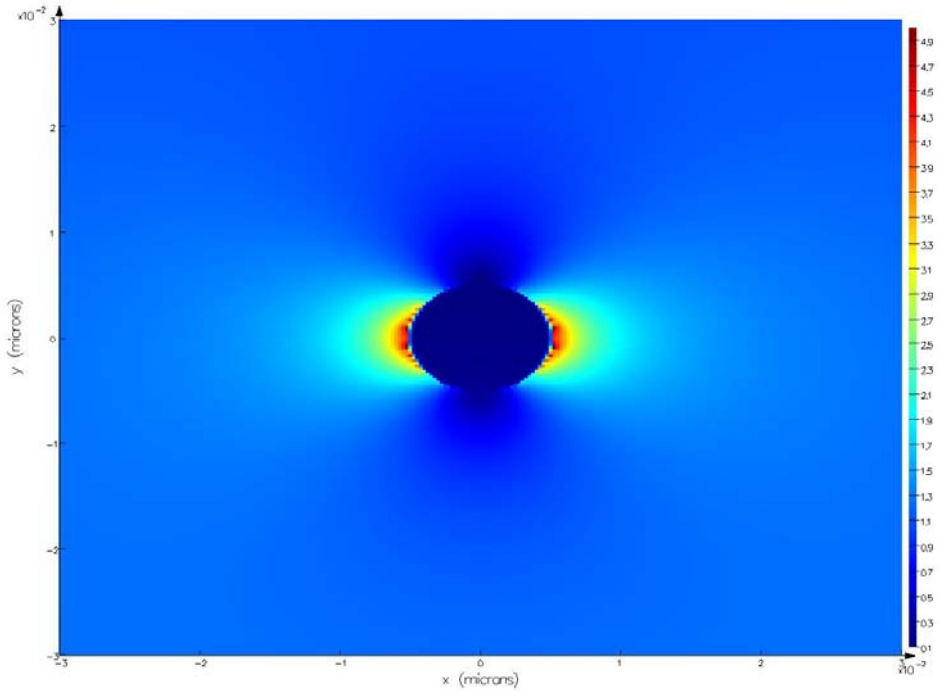

Figure 2.2. Electric field distribution of 10 nm Au metal nanoparticles at an incident plane-wave radiating at 375 nm, propagating along y-axis and polarized along x-axis source.

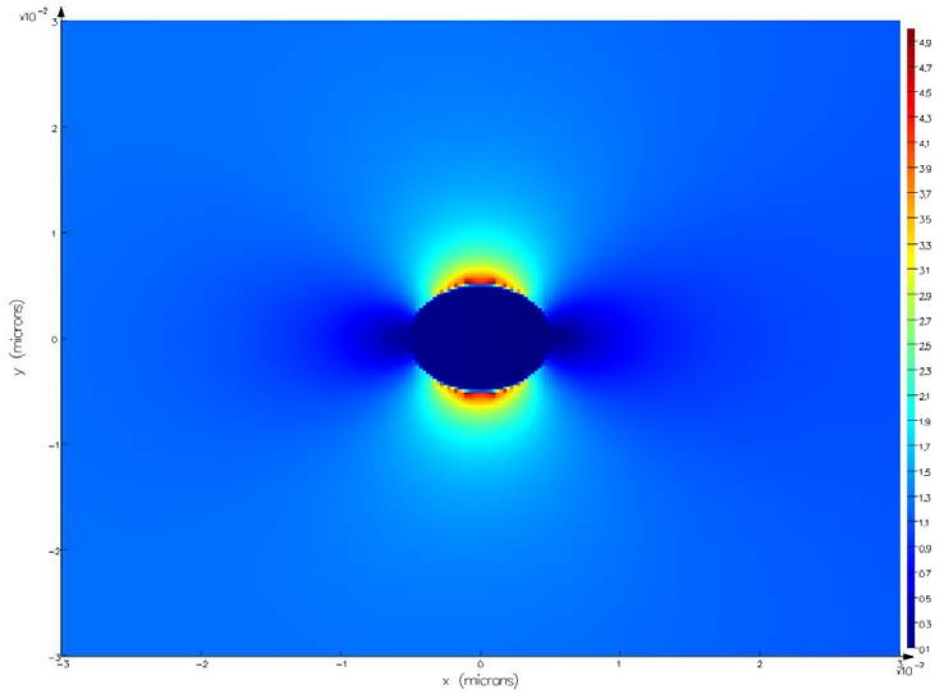

Figure 2.3. Electric field distribution of 10 nm Au metal nanoparticles at an incident plane-wave radiating at 375 nm, propagating along x-axis and polarized along y-axis source.

2.1.2 Size, Shape, Composition and Environment Dependency of Surface Plasmons

Surface plasmon resonance frequency is directly affected by the changes in the size, shape, composition, and environmental factors.

2.1.2.1 Size Dependency

Size dependence on surface plasmon resonance is extensively studied for Au and Ag nanoparticles [23,24]. There are upper and lower size limits for the observation of surface plasmon resonance in such metals. In dimensions smaller than 5 nm and bigger than 100 nm it is nearly impossible to observe plasmonic effects. Especially for the particle size range of 5-50 nm, both of the metals show strong surface plasmon resonances. General resonance wavelength of Au NPs span the range of 500-600 nm whereas Ag NPs span the region between 380-430 nm [25,26]. Increased particle size results in a red shift in the plasmon resonance. In the case of big nanoparticles, the wavelength of the incident radiation becomes comparable to the particle size. This perturbs the surface polarization and results in broadening of the absorption band. Also one of the key factors effective on plasmon resonance spectrum is the monodispersity of size distribution.

2.1.2.2 Shape Dependency

Surface plasmon resonances of metal nanoparticles are strongly shape dependent [27]. There are some reports in the literature for the formation of nanoparticles in different shapes including the conventional spherical one, cubical, one and

cylindrical one. In one of these reports it has been shown that the plasmon resonance wavelength of a spherical Ag NP shifts from 400 to 670 nm by changing its shape to trigonal prism [28]. This is due to the modified boundary conditions of the system corresponding to perturbed collective oscillations of conduction electrons and electromagnetic waves [29]. Additionally with the modification of shape into cylindrical systems (such as nanorods), the effect of polarization of the incident radiation completely changes. There are two types of surface plasmons formed corresponding to the transverse (perpendicular to long-axis) and the longitudinal (parallel to long-axis) components of the resonance.

2.1.2.3 Composition-Environment Dependency

It is also possible to make alloys of metal nanoparticles during their formation. There are also a number of reports in the literature in which plasmon resonance spectrum is shifted with increasing Au or Ag composition in the alloy during the formation of Au-Ag alloy nanoparticles using simultaneous reduction of metal salts [30]. This is also used to tune the surface plasmon resonance wavelength to cover most of the visible spectrum [31].

Another methodology used to alter surface plasmon resonance is the change of surrounding medium. Using different kinds of solvents modify the refractive index of the surrounding or slightly modify the nanoparticle surface. Also the formation of metal-core/dielectric-shell nanoparticles is a well-known method, where the presence of dielectric causes a red shift in the plasmon resonance spectrum [32]. This red shift stems from the increased refractive index of the surrounding medium around the nanoparticle and strongly depends on the shell thickness. At visible wavelengths, the refractive indices of silica, water, and air are ca. 1.45, 1.33, and 1.00 respectively.

2.1.3 Drude Model

Drude model is a useful tool for the prediction of the plasmon resonance frequency under different modifications of a metal nanoparticle system [33,34]. This model depends on the electron density of the system, the dielectric constant of the surrounding, and the effective mass, as given in (2).

$$\omega_p^2 = \frac{ne^2}{\varepsilon_0 m_{eff}} \tag{2}$$

It is demonstrated that by the radiation of UV light incident to the metal nanoparticles, their electron density is increased and, as result, a significant blue-shift in the plasmon resonance wavelength is observed [35]. Also the addition of electron donating agents results in a blue shift and electron accepting agents results in a red shift in the plasmon resonance wavelength, which can be explained using the Drude model.

2.1.4 Metal Nanoparticle Formation

There are many techniques developed to make nanoscale metals including colloidal nanoparticle synthesis, electron-beam lithography, and metal island formation. Electron-beam lithography offers high precision, however this method is the most expensive and time consuming one. In this thesis work, we focus on the use of thermal evaporation techniques to obtain metal nanoislands and colloidal synthesis of metal nanoparticles using chemical reduction method, both of which are simple and low-cost methods.

2.1.4.1 Colloidal Metal Nanoparticle Synthesis Using Chemical Reduction of Metal Salts

There are different kinds of synthetic procedures for metal NP synthesis. One of them is based on the use of a soluble metal salt as the reducing agent. Also to achieve stable nanoparticles in this method, a stabilizing agent is added during or following the synthesis. Reducing agents directly affect the size of metal particles; using stronger reducers result in smaller particles. In a conventional Au NP synthesis $HAuCl_4$ serves as the metal salt and citrate serves as a reducing agent and as a stabilizer as well. The use of citrate provides the formation of spherical Au nanoparticles and negative surface charge [36].

2.1.4.2 Metal Nanoisland Formation Using Thermal Evaporation

Decreasing the pressure of the environment it is possible to evaporate most of the metals even at temperatures close to the room temperature. Using this methodology, in high vacuum chambers, the metal can be heated by an electron beam gun or a thermal resistor until it evaporates. The resulting metal vapor then reaches the surface of a cold substrate on which the film is deposited by condensation of the metal vapor atoms. This method is conveniently used for deposition of thin metal films on substrates. By altering the evaporation conditions, surface morphology of the deposited film can be changed. At very low evaporation rates, a very small amount of the metal vapor arrives at the surface of the substrate and condensates there. Repeating this slow condensation, metal vapors form in the shape of isolated nano-islands instead of continuous films [37,38]. This method is one of the easiest ways of achieving nanoparticles without requiring any synthesis or any lithography procedures.

Chapter 3

Semiconductor Nanocrystals

Semiconductor nanocrystals, also widely known as colloidal quantum dots, are a class of nanoscopic materials typically composed of elements from the periodic table of groups II-VI, III-V and IV-VI. The first comprehensive study that led to the observation of electronic spectra of nanocrystals was conducted in 1937 by Froelich [39]. Quantum size effects of these nanostructures, on the other hand, were found only in the 80s, independent from each other in the United States and in Russia [40,41]. A rapidly growing research on the fundamental physics of quantum dots has been going on since then over the last twenty years, including our research group's work continuing for more than five years now. During this time period of over 20 years, only core nanocrystals containing a broad variety of elements have been synthesized including CdS, CdSe, ZnS, CdTe, PbS, PbSe, Si and Ge [42,43,44,45,46,47,48]. Different from these core structures, there are also core-shell nanocrystals that have been synthesized including CdSe/ZnS [49] and CdTe/CdS [50], as depicted in Figure 3.1 [51]. The material that constitutes the shell structure of the core/shell nanocrystals commonly has a wider bandgap, which serves for the surface passivation and the emission enhancement of those nanocrystals. The increased emission is achieved through the confinement of the charge carriers inside the nanocrystals.

Of particular interest in our research group are colloidal nanocrystals containing the elements cadmium and selenium, which may also be surrounded by a shell composed of zinc and sulphur. Another class of nanocrystals, recently developed for water-based applications, is cadmium telluride nanocrystals of the II-VI groups. Ongoing research makes important progress towards finding new, environment-friendly experimental routes and compounds for quantum dot formation, development of synthesis techniques for better size control and monodispersity, and the integration of these quantum dots into novel structures via surface functionalization (ligand).

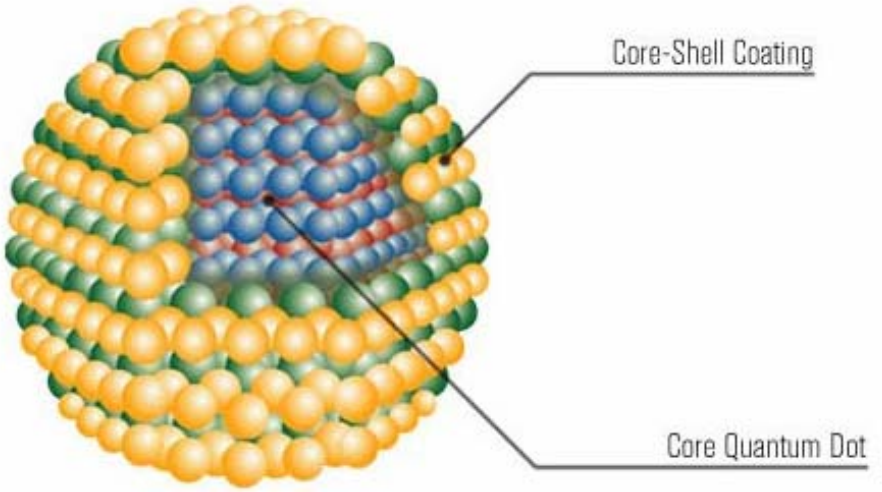

Figure 3.1. Schematic representation of a core-shell quantum structure (Evident Technologies) [51].

The wavelength control of the emitted light resulting from the excitation of nanocrystals is mainly governed by two factors. The first one is the composition of the nanocrystal. The second is the size. Syntheses of semiconductor nanocrystals typically result in the formation of spherical-like crystalline structures with diameters ranging from one to tens of nanometers. This gives rise to the quantum confinement effect. This effect takes place when electrons and holes are trapped in a potential well in the quantum dot in three dimensions. The Bohr exciton radius, which is the size of an exciton in a bulk crystal, here

plays a critical role. The more the dimensions of the nanocrystal approach that of the Bohr radius, the more energy is needed to trap the electron-hole pair within that small volume. This can be understood by the exciton binding energy given in (3).

$$E_n = \frac{\hbar^2 n^2}{8mr^2} \tag{3}$$

This phenomenon commonly known as the quantum size effect is the underlying reason for the blue-shifted emission for decreasing nanocrystal dimensions. In other words, for larger nanocrystals we obtain an emission towards the red end of the visible spectrum, while the emission turns out to be more at the blue side for smaller ones. To give a specific example the emission range covered by CdSe/ZnS core-shell type nanocrystals lies from around 490 nm to 620 nm [49], while for PbSe and PbS this ranges from 850 nm to 2100 nm [46]. Thus, as the main features, variations in size and potential depth as well as in the composition of nanocrystals successfully enable the color tuning of the emission, which makes nanocrystals an ideal material, e.g, for lighting applications in the field of display technologies.

It is worth noting that nanocrystals should be considered different from their bulk forms. In bulk form crystals exhibit more continuous-like energy bands. Energy levels, however, become more discrete when the quantum size effects come into play via reduction of crystal size to nanoscales, by which electron hole pairs are confined to quasi-zero dimensions. Because of their similarity to atoms in terms of quantized energy levels, nanocrystals are also sometimes referred to as “artificial atoms”. Different from atoms, which exhibit very sharp and distinctive absorption and emission spectra, nanocrystals exhibit different emission and absorption characteristics owing to their electronic band structure. Electron and hole states are separated by a forbidden bandgap region in these semiconducting nanocrystallites [52]. The size-dependent quantization in energy

levels, combined with their potentially high quantum efficiencies, makes nanocrystals predominantly an indispensable material for optical applications. The fluorescence quantum efficiency is a measure of how much of the incoming pump light is transformed into the outgoing emitted light (i.e., the number of emitted photons divided by the number of absorbed photons). The highest level for the quantum efficiency of nanocrystals is around 80%.

As quasi-zero dimensional nanostructures exhibit attractive optical properties, numerous application fields of nanocrystals have emerged in the past few years ranging from optical device electronics to biological sciences. In this list one may include the fabrication of light emitting diodes [8], diode lasers [53], storage devices [54], photodetectors [9], photovoltaic solar cells [55], amplifiers [56], and sensors for biological applications [10]. Even solid-state quantum computation for more precise measurements as well as quantum calculations with entangled quantum dots (qubits) are giving shape to future prospects of the potential nanocrystal applications [57].

3.1 CdTe Nanocrystal Synthesis

We synthesize CdTe nanocrystals at our synthesis laboratory. We also closely work with Technical University of Dresden, Germany for our scientific research collaboration and exchange program. Our typical synthesis procedure is as follows under the methodology of our collaborators works [58,59]. In Step 1, we prepare a 0.2 L of Milli-Q water solution with 4.59 g $Cd(ClO_4)_2$. In Step 2, we prepare a solution of 1.31 g TGA with Milli-Q water and complete the total amount of volume in Step 1 (0.2 L) and Step 2 (0.3 L) to be 0.5 L. CdTe NCs grow in a basic environment; they are not stable in acidic solutions. So in Step 3, we set the solution pH to be 12 by adding NaOH (ca. 30 mL, added dropwise after pH exceeds 10) under continuous stirring of the solution (c(NaOH)=1

mol/L). In Step 4, we let Argon to flow into the flask. The main flask is stirred at all the times. Additionally in Step 5, a solution of 10 mL H_2SO_4 ($c(H_2SO_4)$=0.5 mol/L) and 15 mL Milli-Q water are prepared in another flask. To pull out the rest of air in this solution, it is bubbled with Argon flow for 20-30 minutes. Then in Step 6, 0.8 g Al_2Te_3 is put into another flask in a glovebox. This requires using the glovebox since Al_2Te_3 is highly attracted and oxidized with air. Constructing an apparatus shown in Figure 3.1.1, the solution of Step 3 (in the big flask on the left) and the material of Step 6 (in the small flask on the right) are connected to each other. Argon is used as the carrier gas during reaction from Al_2Te_3 containing flask to main flask and this Ar flow continues for 30-40 minutes.

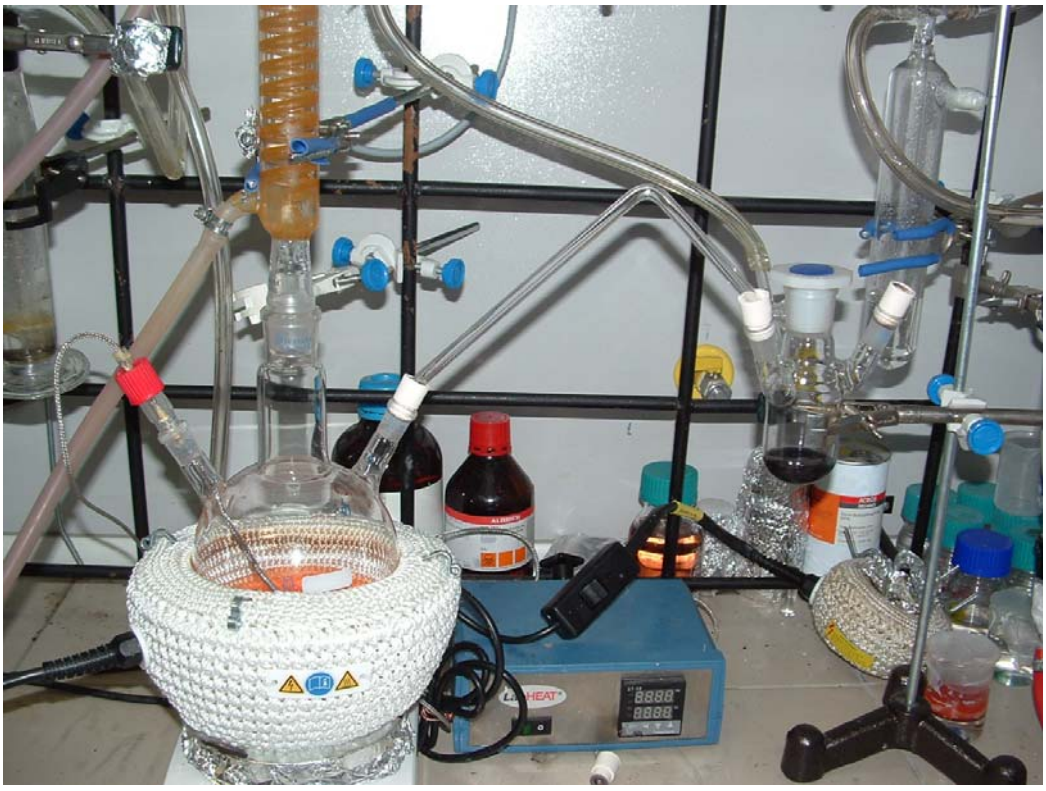

Figure 3.1.1. A picture of CdTe nanocrystal synthesis setup. Precursors are produced in the main flask (left) and Al_2Te_3 source is activated in the small three-necked flask (right).

During the synthesis, we take a 10 mL of Step 5 solution with a syringe and slowly drop into Al_2Te_3. At this stage, the main solution turns into red and then

to a very dark red, finally followed by black color. Up to this step, we do not heat the solution; these steps are only used for the preparation of the pre-cursors. Under stirring, we wait for 25 minutes and then increase the Ar flow. Al_2Te_3 line is removed from the system and the cooler is connected. Using the heater we set the temperature to be 100 ^{0}C. Nanocrystals starts to grow as the mixture starts boiling and gets bigger in size during boiling period. In the first minute NCs are blue then turns into the green and as we wait long enough , we can achieve red color as can shown in Figure 3.1.2. when the mixture is the cooled down rapidly, the reaction is stopped. Using this procedure highly efficient (>50%) and negatively charged CdTe NCs can be synthesized. A picture of our synthesized CdTe NCs under UV light illumination is depicted in Figure 3.1.3. To remove the extra amount of solvent we use a rotary evaporator and increase the NC concentration in solution. Materials are further cleaned from impurities by using paper filters, and size-selectively precipitated after successive centrifugation steps.

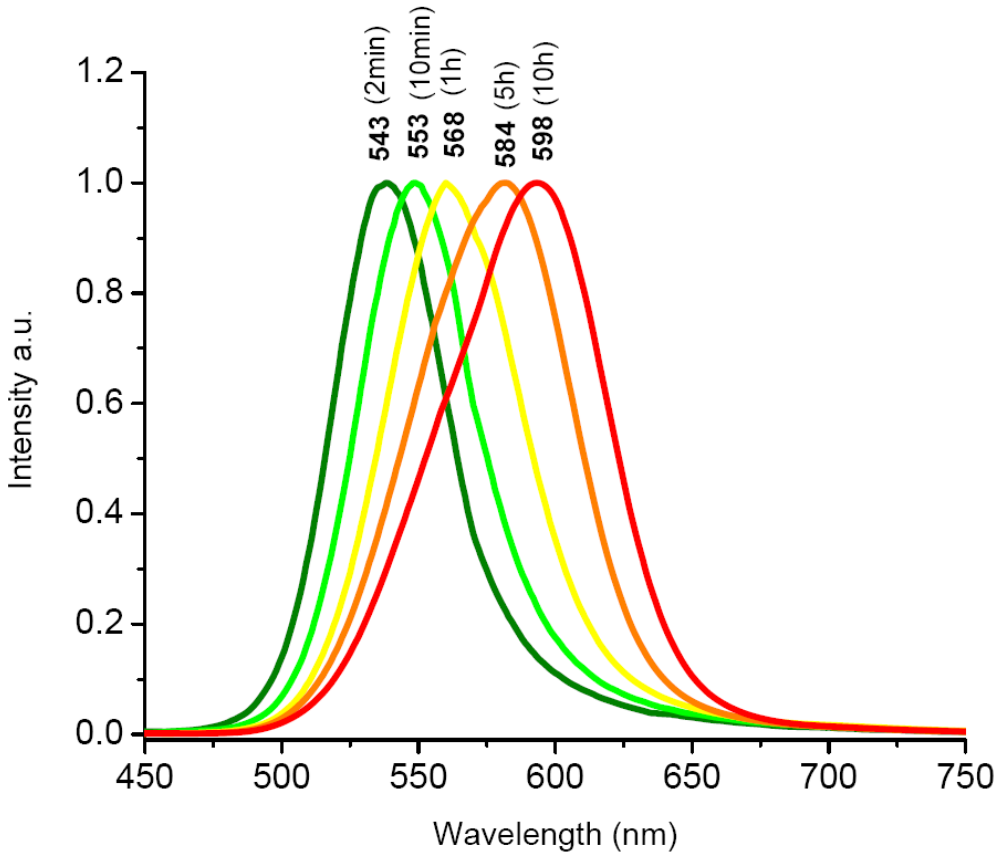

Figure 3.1.2. Normalized photoluminescence spectra of our CdTe NCs emitting at different wavelengths which correspond to different boiling durations.

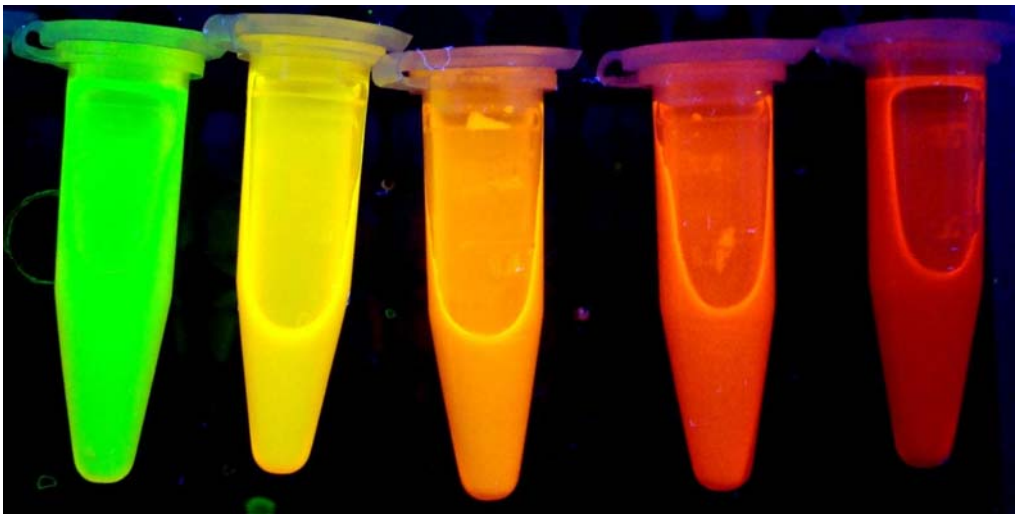

Figure 3.1.3. A picture of our CdTe nanocrystals synthesized to emit at different colors by increasing the boiling duration.

3.2 Quantum Efficiency Measurements

Quantum efficiency of nanocrystals, also known as fluorescence quantum yield, corresponds to the ratio of the number of the absorbed photons to the number of the emitted photons [60]. In such measurements there is a reference material for which we exactly know its quantum efficiency in a specific solvent. Here we use Rhodamine 6G and dissolve it in pure ethanol. The concentration of Rhodamine 6G is very dilute (such that the peak maximum of the absorbance peak is less than 2). We also take the absorbance spectrum of our NCs and set the concentration such that the intersection between the NC and Rhodamine 6G absorbance falls between 460-480 nm). Subsequently, right at this intersection wavelength, we excite both of the solutions of our NCs and the reference Rhodamine using a fluorometer to compare their fluorescence spectra. The emission wavelength (in the x-axis) is converted into energy (eV) simply using

$$E = \frac{hc}{\lambda} \tag{4}$$

where E is the energy, h is the Planck's constant, c is the speed of light, and λ is the wavelength. We then integrate the whole emission spectra for both NC and Rhodamine 6G. Finally, by setting the area of Rhodamine to 95% efficiency, we calculate the quantum efficiency of NCs using its integrated spectral emission area.

An exemplary calculation for one of our CdTe nanocrystals is described below. First we take the absorption spectra for both of the fluorophores. By dissolving 3 μL of our NC in 2 mL of Milli-Q water we obtain the intersection of the absorbance spectra of our NCs and that of the reference Rhodamine at 469 nm, as depicted in Figure 3.2.1.

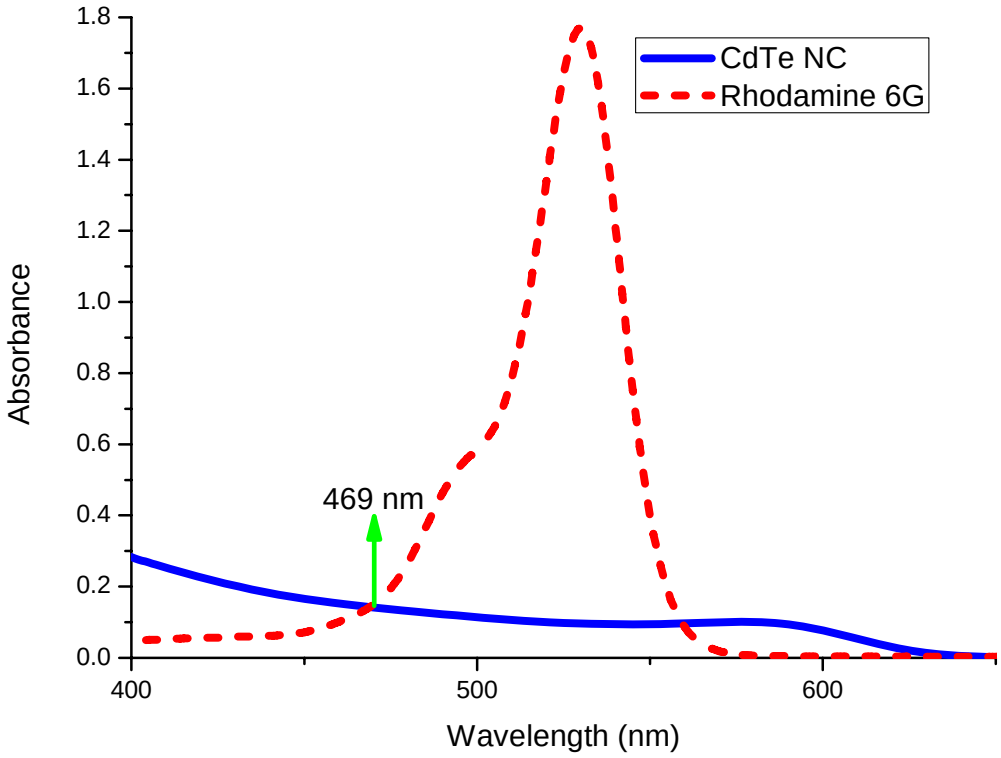

Figure 3.2.1. Absorbance spectra for our CdTe NC and Rhodamine 6G.

We then take emission spectra of both fluorophores at the same excitation wavelength of 469 nm. Figure 3.2.2 shows the emission spectra of these fluorophores in terms of energy values. Integrating both spectral emission areas using Origin 7.5, the ratio of CdTe to that of Rhodamine 6G area is calculated to be 0.43. Since we know that Rhodamine 6G has a quantum efficiency of 95%, we obtain the quantum efficacy of our CdTe NC to be approximately 41% in solution.

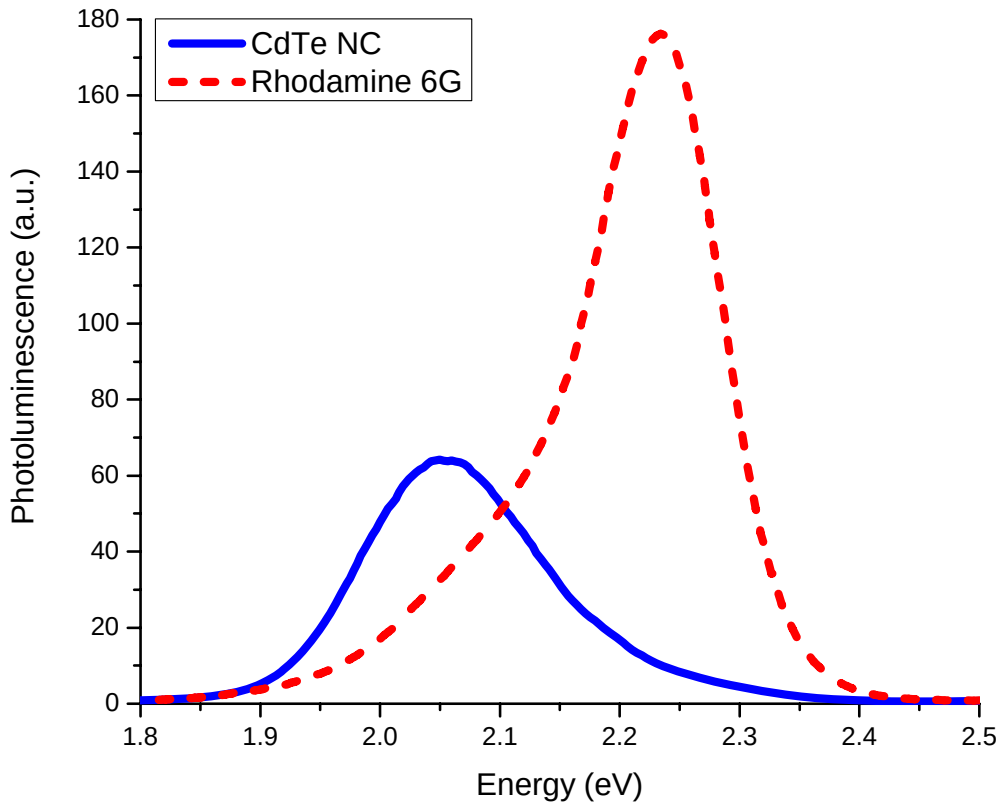

Figure 3.2.2. Photoluminescence emission spectra for our CdTe NC and Rhodamine 6G excited at 469 nm.

Chapter 4

Plasmon Enhanced Emission of Nanocomposites Made of Colloidal CdTe nanocrystals and Au nanoparticles in a Repeating Layered Architecture

4.1 Metal-Enhanced Fluorescence of Nanocrystal Films

In the last few decades, there has been a great interest in the investigation of photo-physical properties of surface plasmons, which significantly modify radiative and non-radiative decay rates of fluorophore photoluminescence [12]. Such plasmonic effects are applied to light generation and light harvesting. Also, colloidal semiconductor nanocrystals have attracted great attention for their

potential use in different applications including solid-state lighting [8], photovoltaics [9], and bio-labeling [10]. The use of nanocrystals in such applications necessitates the investigation of obtaining highly efficient NC solids. However, the quantum efficiency of colloidal NCs unfortunately decreases with the film formation [11]. For this, metal-enhanced luminescence provides a potential solution to obtain higher levels of optical emission from these nanocrystals in film via plasmon coupling. The emission intensity of nanocrystals can be highly modified by the oscillating plasmons of metal nanoparticles (NPs) when brought into close proximity. Nanocrystal emission can be enhanced (or quenched) via plasmonic coupling due to the increase in the radiative (or non-radiative) decay rates under certain conditions. Separation between metal nanoparticles and nanocrystals, spectral match between plasmon resonance wavelength of metal nanoparticles and emission wavelength of nanocrystals are among important conditions affecting nanocrystal emission mechanisms.

4.2 A New Three-Dimensional Nanocomposite Structure for Plasmon-Enhanced Emission of Colloidal CdTe Nanocrystals Using a Repeating Layered Architecture

In the literature, plasmonic coupling of nanocrystals using plasmonic metal nanoparticles have been previously demonstrated [13,14,15]. One of the main methods used for such plasmonic coupling is the use of layer-by-layer coating of metal nanoparticles and nanocrystals. Previous works focused only on the plasmonic coupling of bilayers that contain the NC films located at the top or the

bottom of the metal nanoparticle films. Here we instead show plasmonic coupling of nanocrystals in a three-dimensional construction by repeating unit cells of semiconductor NC and metal nanoparticle bilayers. This approach holds great promise for the development of optoelectronic device technology to embed plasmonic nanoparticles and NC composites for the demonstration of highly efficient emitters and absorbers.

In this work, we increase the quantum efficiency of NCs in the composite film using plasmon enhanced colloidal nanocrystal solids integrated with Au NPs in close proximity within a repeating architecture. Here three different unit cells are prepared with the combinations of plasmonic Au NP monolayers, CdTe NC monolayers, and dielectric spacer monolayers (MLs). The prepared unit cells are repeated for 2, 3 and 5 times for a comparative study of the increased repetition of unit cells. For the best plasmonic coupling condition, we synthesize Au NP and CdTe NC at specific sizes to spectrally match the plasmonic resonance of Au NP to the absorption and emission peak wavelengths of the NCs. Then the dielectric spacer thickness between the nanocrystals and metal nanoparticles is optimized to get the maximum emission enhancement between them. We observe that emission of NC layers is enhanced as their fluorescence decay lifetimes are shortened by repeating our optimized unit cell architecture.

4.3 Nanostructure Preparation

In our experiments we synthesize all of the nanocrystal and metal nanoparticle materials to have large amounts of material to reproduce each experimental result. Additionally, this introduces flexibility to tune the NC emission wavelength and Au nanoparticle plasmon resonance wavelength by modifying our synthesis recipes. This wavelength tuning ability is crucial in the demonstration of plasmonic applications since there has to be a spectral match between the plasmon resonance wavelength and fluorescent emission

wavelength. Our nanocrystals are synthesized using the procedure described in Chapter 3. Below is the procedure for the synthesis of Au nanoparticles.

We prepare our gold colloids using chemical reduction method. For that, we use Chloroauric acid $HAuCl_4$ (Sigma Aldrich, UK) and trisodium citrate $Na_3C_6H_5O_7$ (Sigma Aldrich, UK) of analytical grade purity, as the starting materials without further purification. In Step 1, 0.08 g of Chloroauric acid is dissolved in 200 mL of Milli-Q water corresponding to a molarity of 1 mM.. In Step 2, 0.26 g of Sodium citrate is dissolved in 20 mL of Milli-Q water corresponding to a molarity of 44 mM in another beaker. Under continuous stirring, the first beaker is heated up until it starts boiling. Sodium citrate solution in the second beaker is added quickly into the first beaker. The mixture is boiled for 20-30 minutes to obtain stable dispersion of dark-red colored gold nanoparticles. Finally, the mixture is cooled down to room temperature under continuous stirring, as shown in Figure 4.3.1.

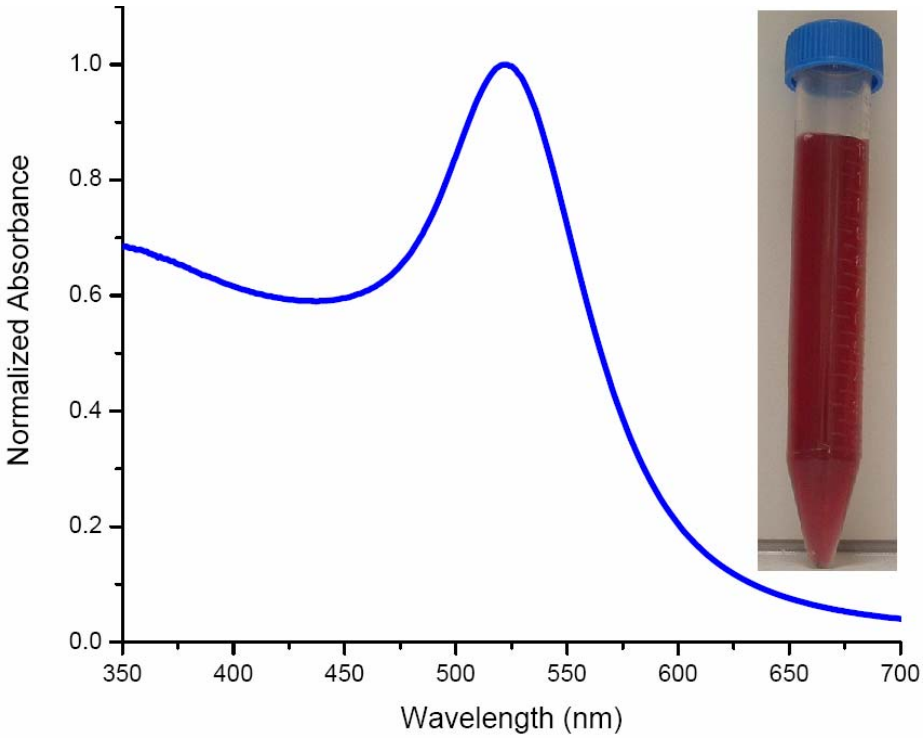

Figure 4.3.1 Optical absorption spectrum of our Au nanoparticles. Inset is a picture of our Au nanoparticles in vial after synthesis.

The absorption spectrum of our Au colloids is obtained with a peak maximum at 520 nm with a full width half maximum of around 80-90 nm as depicted in Figure 4.3.1. This synthesis results in an average particle size of 15 nm with an expected size dispersion of 10% as shown in Figure 4.3.2.

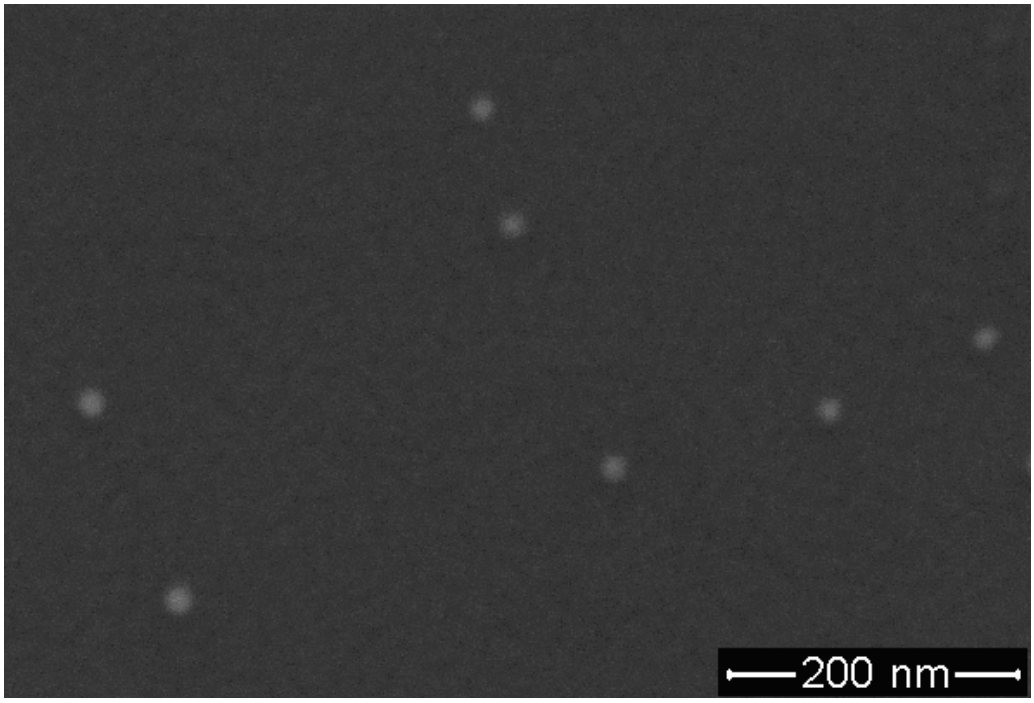

Figure 4.3.2. Scanning electron microscopy image of our diluted Au nanoparticles.

4.4 Layer-by-layer Film Deposition

We construct composite films of our hybrid structures (semiconductor NCs and metal NPs) in layer-by-layer assembly using a computerized dip coater system manufactured by Nima Technology, UK, shown in Figure 4.4.1. For LbL construction, 2mg/mL of positively charged polymer, poly(diallyldimethylammonium chloride) (PDDA) is dissolved in 0.1 M NaCl solution, coated on negatively charged Corning glasses, and used in all NC monolayers and Au nanoparticle constructions. Poly(styrene sulfonate) (PSS) is used as the complementary negatively charged polymer with the concentration of 2 mg/ml dissolved in 0.1 M NaCl solution, for dielectric spacing construction.

Figure 4.4.1. Picture of our dip-coater system at Bilkent Demir Lab.

4.5 Experimental Demonstration and Optical Characterization Results

We first optimize our system as a metal-dimer system of two metal NPs since the plasmonic effects are modified with respect to one side coupled system, as

derived from numerical and experimental results. Our FDTD calculations show that due to coupling effect of metal nanoparticles, as the number of metal nanoparticle layers electric field intensity between each metal nanoparticle increases as depicted in Fig. 4.5.1 and 4.5.2.

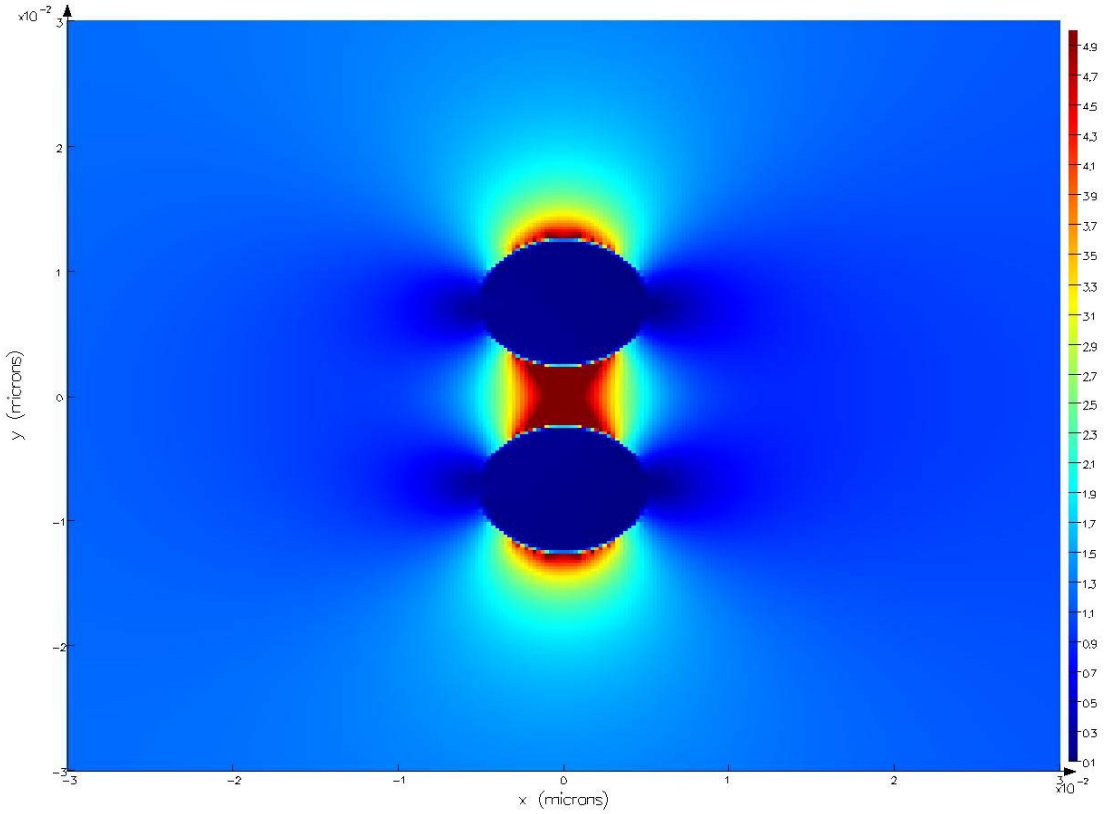

Figure 4.5.1. Electric field distribution of 2 vertically aligned 10 nm Au metal nanoparticles at an incident plane-wave radiating at 375 nm, propagating along x-axis and polarized along y-axis source.

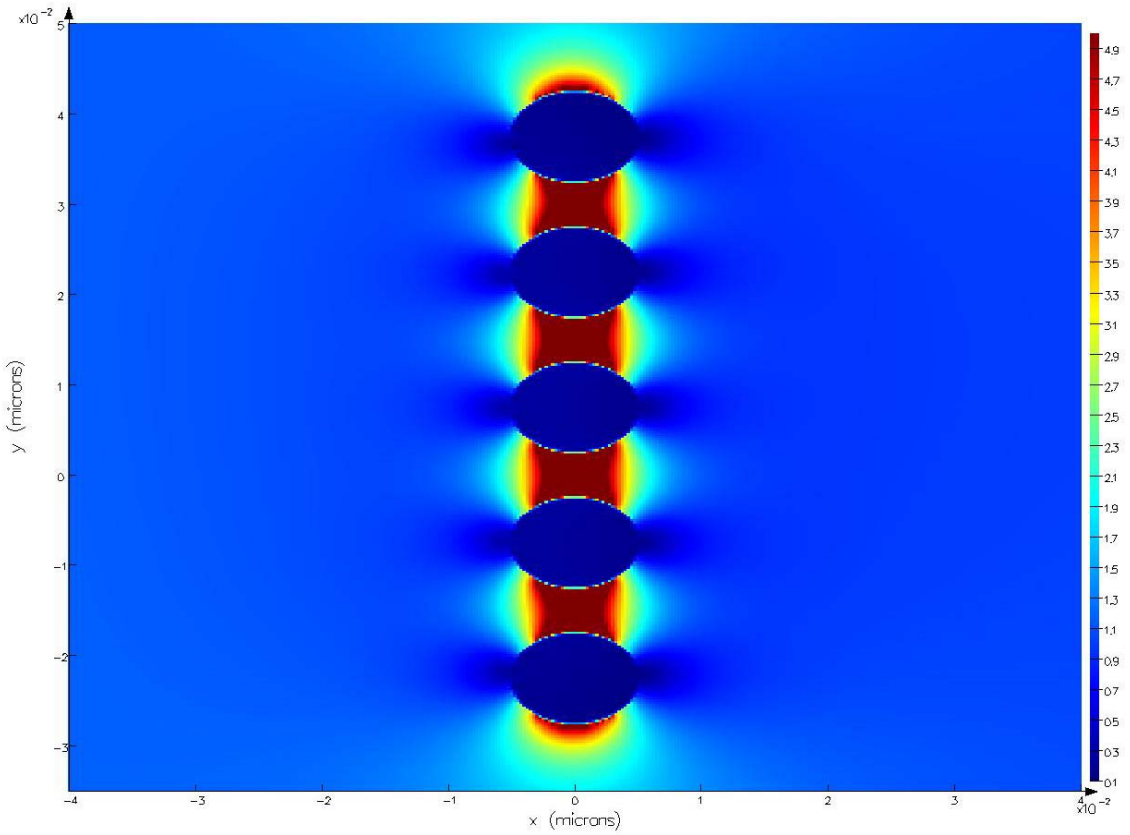

Figure 4.5.2. Electric field distribution of 5 vertically aligned 10 nm Au metal nanoparticles at an incident plane-wave radiating at 375 nm, propagating along x-axis and polarized along y-axis source.

For the experimental demonstration, from our previous results we observe that a spacing of 6-8 MLs is optimal for emission enhancement between a single Au NP ML and NC ML. However, the optimal spacing decreases down to 3-4 MLs for NC ML sandwiched between two Au NP MLs. In this direction, the first sample set is constructed with a unit cell consisting of 3 MLs of negatively charged NCs coated with positively charged PDDA. On top of NC layers, 3 MLs of PDDA/PSS coated to serve as a dielectric spacer. This first set (named NC) serves as the reference emission level coming only from CdTe NCs and a representative schematic is shown in Figure 4.5.3.

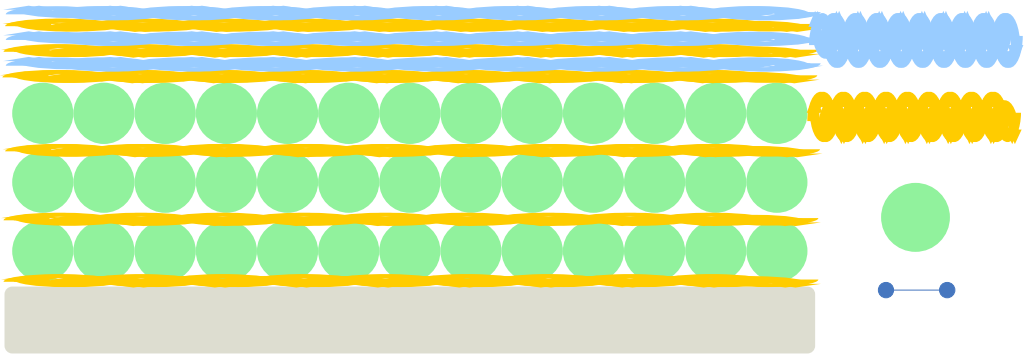

Figure 4.5.3. Schematic representation of the first unit cell that contains only CdTe NCs and a dielectric spacer.

The second sample set (named Au-NC) consists of 3 MLs of Au NPs followed by coating of 3 MLs of NCs with no spacer layers. This set serves for the investigation of PL quenching due to the direct contact to the metal NPs; a representative schematic is shown in Figure 4.5.4.

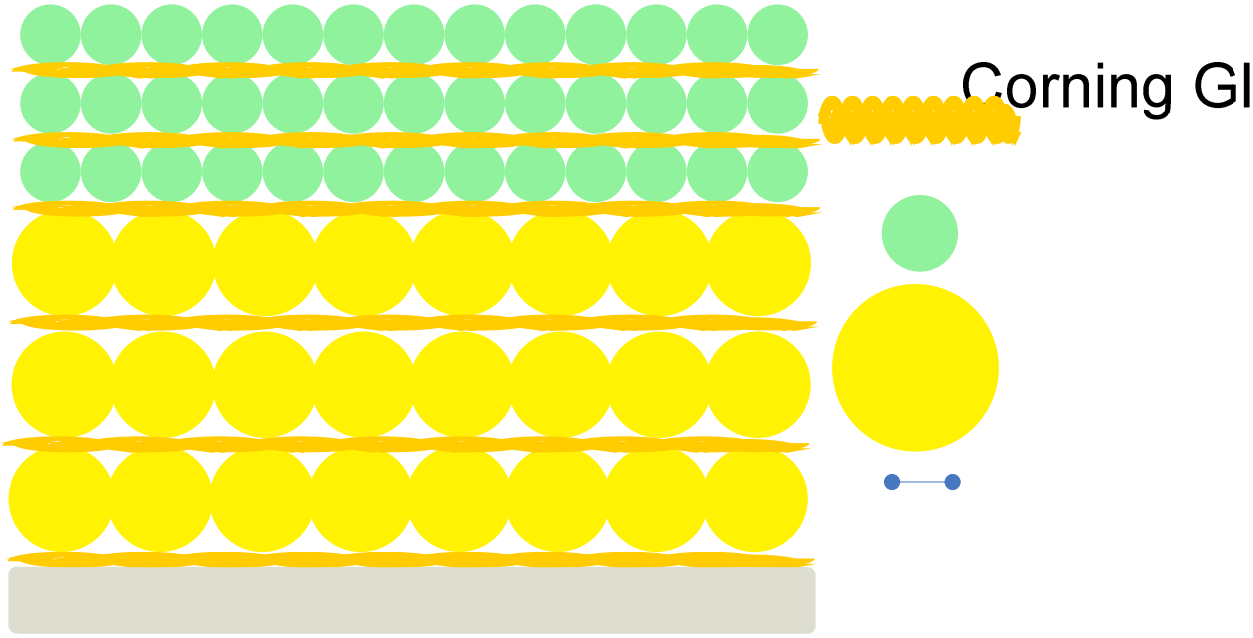

Figure 4.5.4. Schematic representation of the second unit cell that contains Au NPs and CdTe NCs with no spacer.

The third sample set (named Au-spacer-NC) consists of 3 MLs of Au NPs, followed by the dielectric spacer of 3 MLs of PDDA/PSS bilayers, and 3 MLs of NCs. A representative schematic of this composite structure is shown in Figure 4.5.5. Also pictures of Corning glasses samples (coated with each unit cell repeated for 3 times for the NC-spacer, Au-NC, and Au-spacer-NC, respectively) are given in Figure 4.5.6.

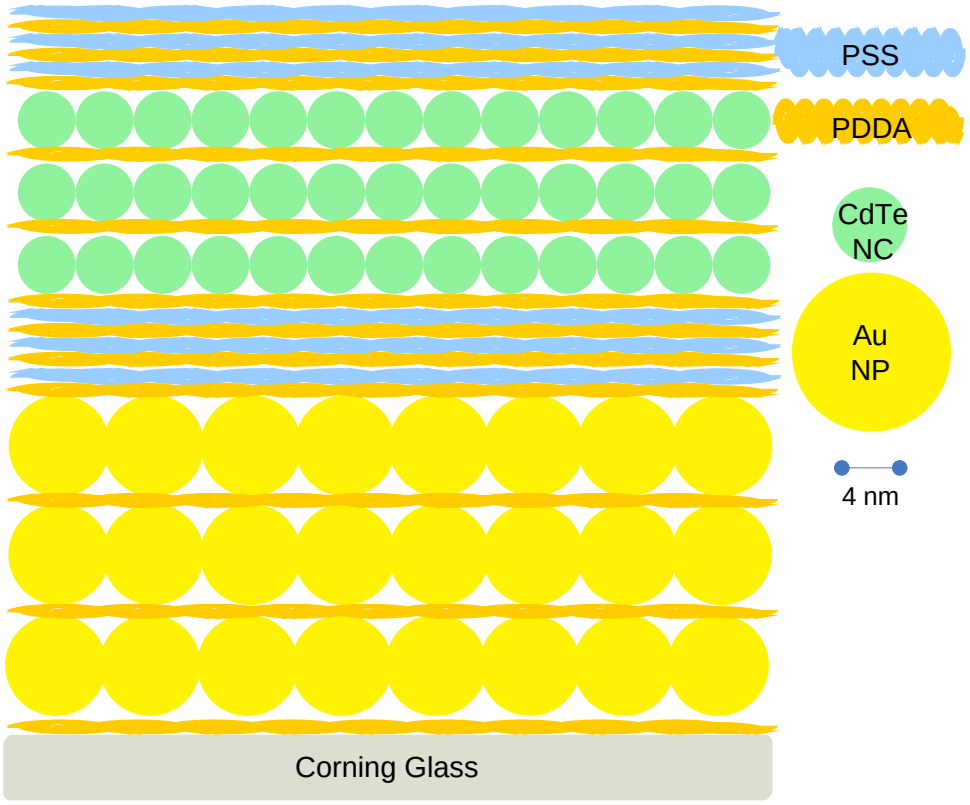

Figure 4.5.5. Schematic representation of the third unit cell that contains Au NPs, CdTe NCs, and a dielectric spacer.

Here we experimentally find out that 3 MLs of PDDA/PSS bilayers make the optimal dielectric spacing for the enhancement of NC emission in our case. This enhancement factor is measured to be 2 only for one unit cell. This enhancement factor is not very high compared to some of previously reported works since we start with efficient nanocrystals. The room for photoluminescence enhancement

inversely depends on the starting quantum efficiency of the nanocrystals as described in [12]. So starting with a low-efficiency nanocrystal, it is possible to obtain much higher enhancement factors.

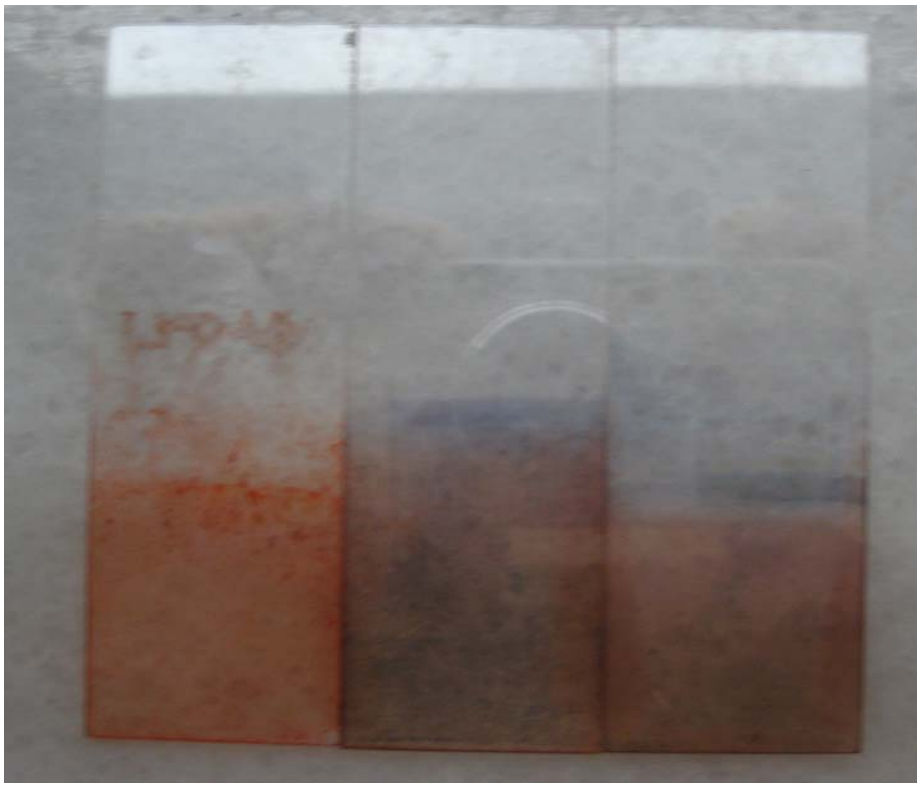

Figure 4.5.6. Pictures of Corning glasses samples coated with each unit cell repeated for 3 times for NC, Au-NC, and Au-spacer-NC, respectively (placed side by side in the given order here).

Photoluminescence spectra of 2, 3, and 5 times repeated unit cells of Au NP and CdTe NC nanocomposite films are depicted in Figure 4.5.7 (a), (b), and (c), respectively. We observe that, in the presence of metal NPs separated by dielectric layer, NC emission is significantly enhanced. But in the presence of metal NPs lacking a dielectric spacer, NC emission is quenched. We calculate that the NC emission is enhanced by a factor of 3.55 with 2 unit cells repetition. 3 unit cells repetition results in an enhancement factor of 4.17. For 5 unit cells, the highest emission enhancement is observed with a factor of 4.37.

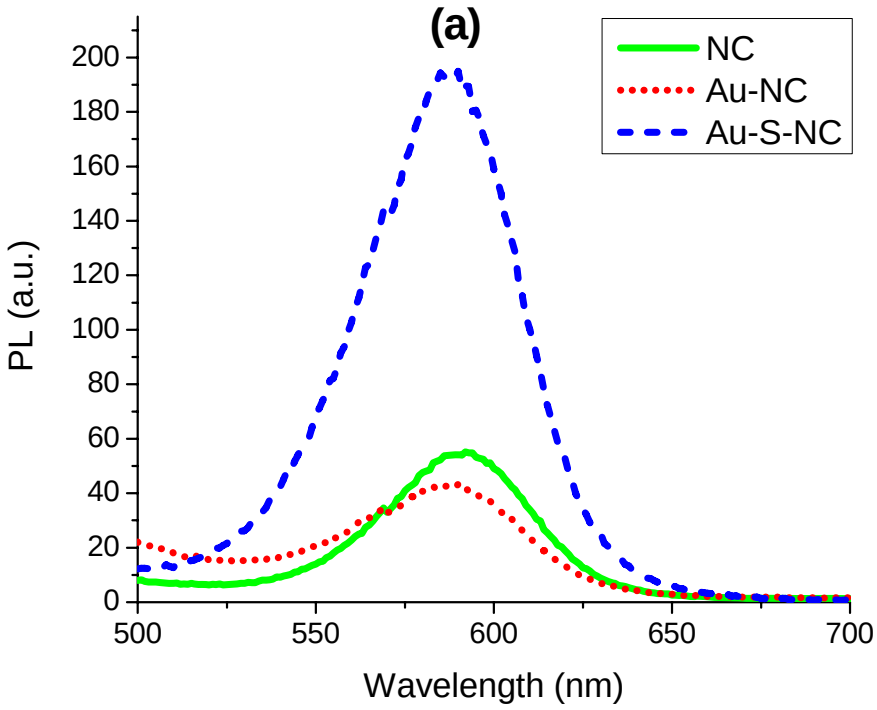
(a)
NC
Au-NC
Au-S-NC
PL (a.u.)
0
20
40
60
80
100
120
140
160
180
200
500
550
600
650
700
Wavelength (nm)

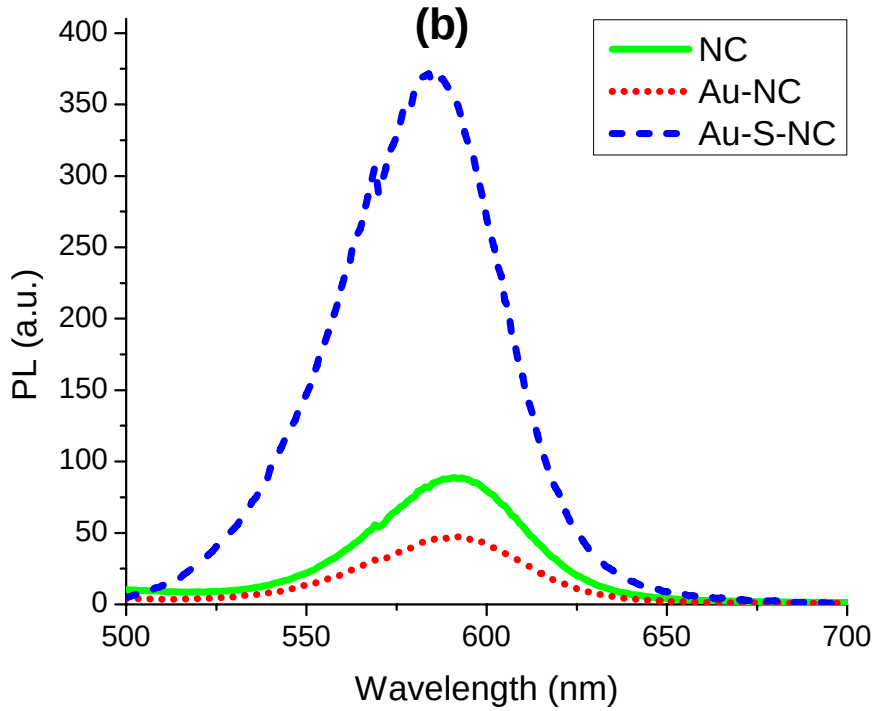
(b)
NC
Au-NC
Au-S-NC
PL (a.u.)
0
50
100
150
200
250
300
350
400
500
550
600
650
700
Wavelength (nm)

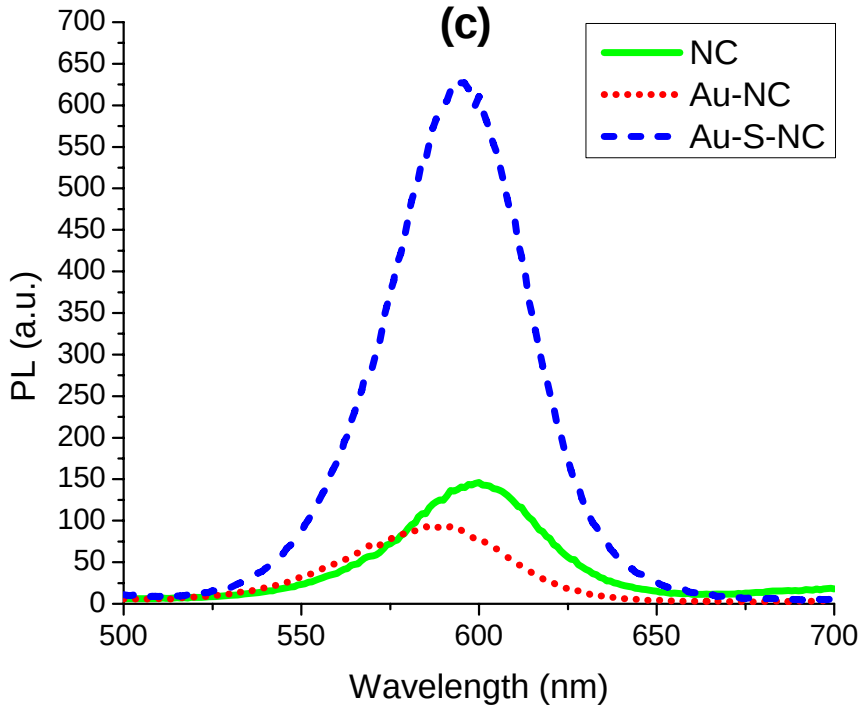

Figure 4.5.7. PL spectra of our CdTe NCs alone (NC) and those in the presence of Au NPs (Au-NC) and in the presence of Au NPs and a dielectric spacer (Au-S-NC), with their CdTe NC - Au NP unit cell repeated (a) 2, (b) 3, and (c) 5 times in the composite.

We use an integrated sphere that is connected to an optical power meter and an optical spectrum analyzer to observe the change in the emission characteristics of these composite samples. Using this setup, we measure the starting quantum efficiency of our NC films alone to be 19% (whereas quantum efficiencies as low as only few percents are common for NCs in solid films in the literature). In the case of Au-CdTe nanocomposite films, using Au nanoparticles at the fixed optimal dielectric spacing, we increase this film quantum efficiency to a high level of 30% in film by repeating the unit cells five times, which is the highest film quantum efficiency reported for CdTe NCs in film in the literature, to the best of our knowledge. This corresponds to a quantum efficiency enhancement of 63%.

We also comparatively investigate emission kinetics of these samples by taking time-resolved fluorescence decay curves, as depicted in Figure 4.5.8. We observe a significant shortening in decay time for each set of Au NP and CdTe NC films. For the most enhanced emission (of the unit cells repeated for 5 times), the photon decay lifetime of CdTe NCs is modified from 7.92 ns to 1.82 ns in the presence of metal NPs and to 2.84 ns in the presence of metal NPs separated with dielectric layers.

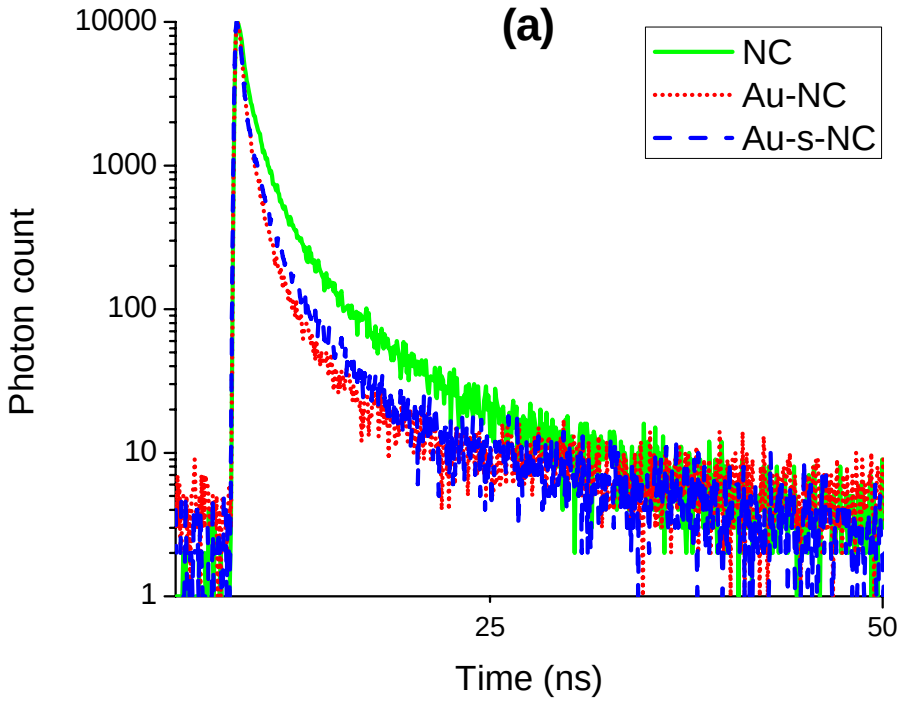

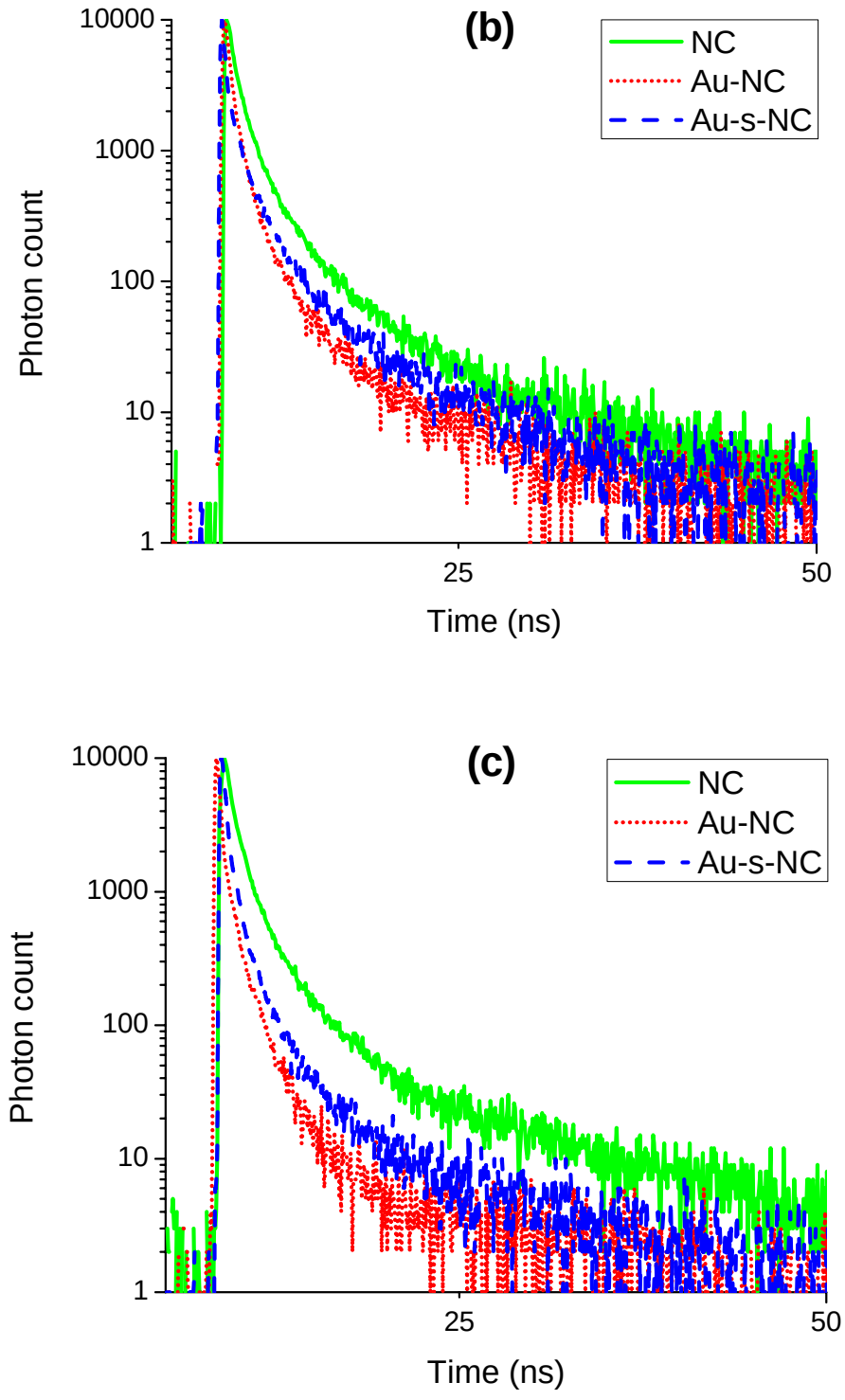

Figure 4.5.8. Time resolved PL decays of our CdTe NCs alone (NC) and those in the presence of Au NPs (Au-NC) and in the presence of Au NPs and a dielectric spacer (Au-S-NC), with their CdTe NC - Au NP unit cell repeated (a) 2, (b) 3, and (c) 5 times.

Photoluminescence and time-resolved fluorescence characteristics support each other. In both cases with metal NPs, radiative and non-radiative decay rates increase. However, their modified emission spectra can be explained by increased non-radiative decay rate in the presence of metal NPs that results in quenched fluorescence and increased radiative decay rate in the presence of metal NPs separated by dielectric layers that results in enhanced fluorescence.

Enhanced emission due to the repeating structures can be further investigated by the comparison of nanocrystal decay rate with and without Au nanoparticles. For nanocrystals the quantum yield can be expressed in terms of the radiative decay rate to the total physical decay rate including radiative and non-radiative decay components given in (5)

$$Q_0 = \frac{\Gamma}{\Gamma + k_{nr}} \tag{5}$$

where Γ is the radiative decay rate and k_{nr} is the non-radiative decay rate.

In the presence of metal nanoparticles, radiative and non-radiative components are modified and the resulting quantum yield is given in (6)

$$Q_m = \frac{\Gamma + \Gamma_m}{\Gamma + \Gamma_m + k'_{nr}} \tag{6}$$

where Γ is the radiative decay rate, Γ_m is the radiative decay rate in the presence of metal NP, and k'_{nr} is the modified non-radiative decay rate in the presence of metal nanoparticles. Using decay lifetimes of 7.92 ns for the nanocrystals and 2.84 ns in the presence of metal NPs, we calculated Γ_m to be 0.226 ns^{-1}. Also the use of initial quantum yield (0.11) of nanocrystal layers, the radiative decay rate

is calculated to be 0.014 ns^{-1}. Finally, the quantum yield is calculated to be 0.682 in the presence of Au NPs. This corresponds to an enhancement factor of 6.20 in terms of quantum yield comparison. This enhancement factor is close to the experimentally observed enhancement factor of 4.37 under the steady-state conditions.

Finally, we demonstrate the increased efficiency of Au-CdTe nanocomposite films by using a three-dimensional construction of repeating layers. In the 5 times repeating unit cell structure of Au and CdTe nanocomposite film separated by a dielectric layer, there is a significant enhancement of CdTe NC emission by a factor of 4.37, with the enhanced quantum efficiency reaching a level of 30% in film. Our results hold great promise for the development of highly efficient NC-based optoelectronic devices by the use of repeating unit cell architecture.

Chapter 5

Selective Enhancement of Surface-State Emission and Simultaneous Quenching of Interband Transition in White-luminophor CdS Nanocrystals Using Localized Plasmon Coupling

5.1 Metal-Enhanced Fluorescence

Emission from fluorescent materials can be modified by metals in their close vicinity due to plasmonic effects. Using different kinds and sizes of metals the emission enhancement has been demonstrated on many fluorescent materials such as organic dyes and semiconductor nanocrystals.

The presence of metal modifies the radiative and non-radiative recombination rates of fluorescent materials since radiating dipole from the fluorophore and plasmons from the metal interacts with each other. This interaction can modify

the emission mechanism in the near field, which corresponds to creation of high electric fields in the close vicinity of metal.

5.2 Surface-State Emitting Nanocrystals

Recently, our collaborators from Technical University of Dresden, Germany have synthesized CdS nanocrystals with tiny dimensions of 2.4 nm [61]. These NCs have a very high surface-to-volume ratio, which results in a significant modification in their emission states. In addition to the interband transition state from conduction band to valance band, there also exist many trap-states that lead to a wide spectral range of emission from these NCs.

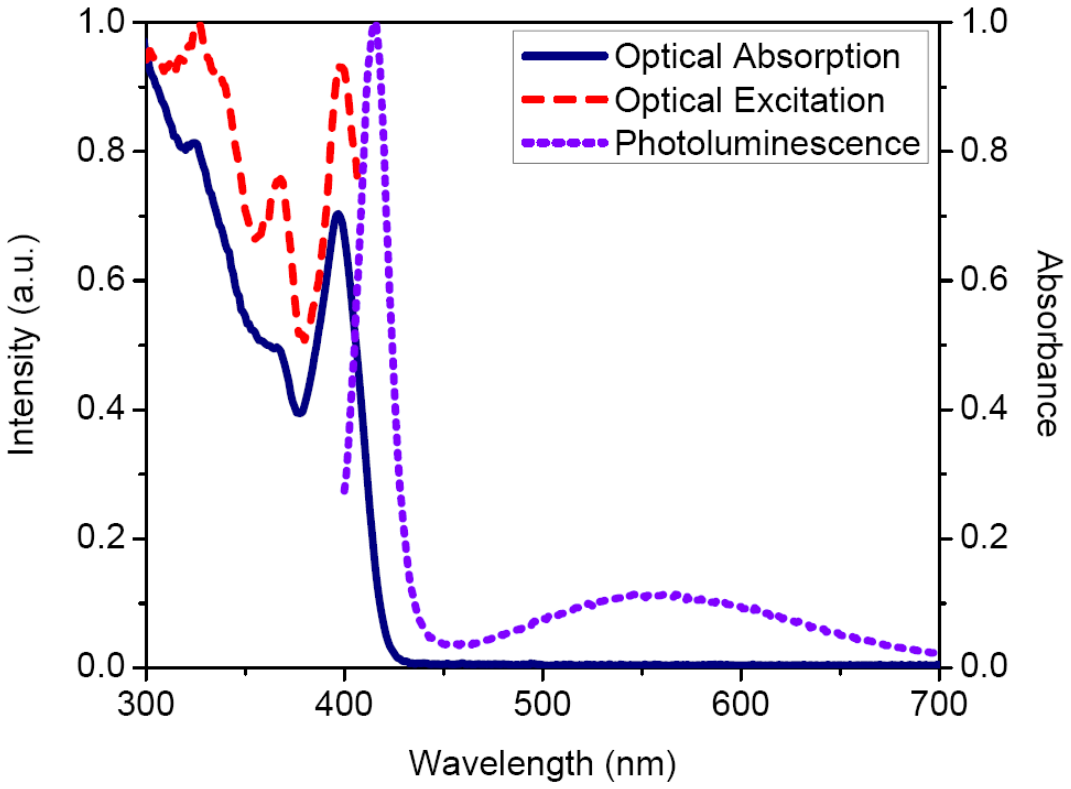

Figure 5.2.1. Optical absorption, optical excitation (for emission maximum at 415 nm), and photoluminescence spectra (excited at 396 nm) of our trap-rich CdS nanocrystals in colloidal form.

Figure 5.2.1 shows the optical absorption and excitation (for emission maximum). These measurements show that first excitonic peak of these NCs is at 396 nm. Figure 5.2.1 also shows the photoluminescence measurements in which the stronger peak due to interband transitions is at 405 nm and the weaker but wider emission due to surface states is at 550 nm. Figure 5.2.2 shows an illustration of emission from the conduction band (CB) to the valance band (VB) for the band-edge (interband) transition and through the mid-gap trap states for the surface-state emission. The wide spectral range of emission covering the entire visible spectrum results in white light generation from such a single type of nanocrystal. Figure 5.2.3 represents photographs of white light emission from surface-state emitting CdS NCs in colloidal form (left) and in film form (right) under UV light exposure.

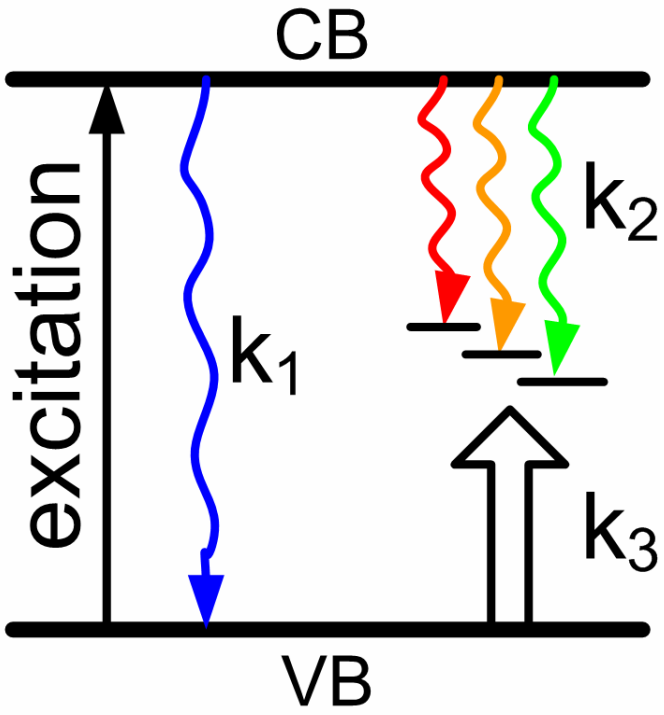

Figure 5.2.2. Schematic illustration of emission from the conduction band (CB) to the valance band (VB) for the band-edge (interband) transition and through the mid-gap trap states for the surface-state emission.

Unfortunately the surface state emission from these NCs is much weaker (8.9 times) than their band-edge emission, which needs to be improved for solid state lighting applications. Additionally, quantum efficiency of these NCs is 17% in colloidal form; however, their quantum efficiency significantly drops when spin cast into films.

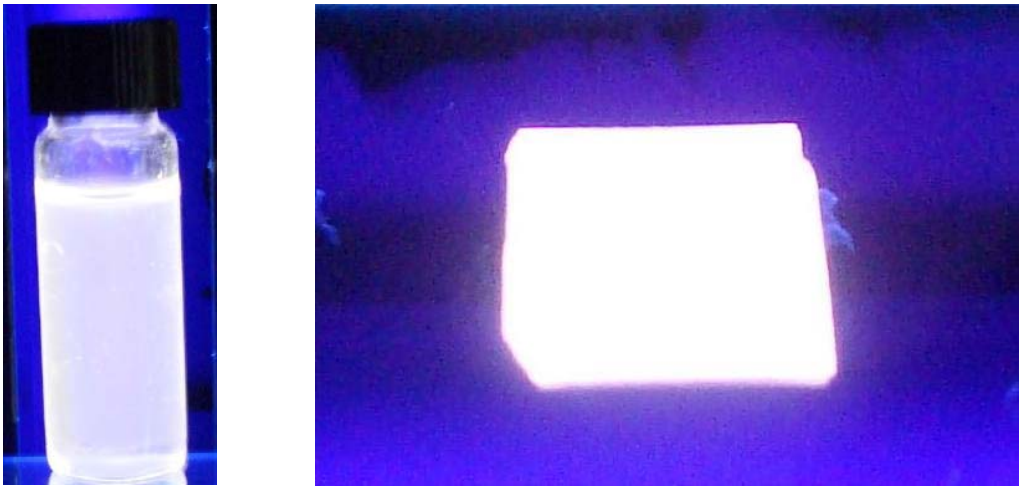

Figure 5.2.3. Photographs of white light emission from trap-rich CdS NCs in colloidal form (left) and in film form (right) under UV light illumination.

5.3 Metal Nanostructures Preparation

We thermally evaporate Ag nano-island films on pre-cleaned quartz substrates in a high vacuum environment at low evaporation rates (0.1-0.2 Å/sec) with film thicknesses below 25 nm. Using high evaporation rates and film thicknesses, flat metal surfaces are obtained. However, with low evaporation rates and mass thicknesses, metals are formed in the forms of randomly separated islands with a few nanometers of diameters. We use a rapid thermal annealer to obtain bigger nanoparticles with higher optical densities. During annealing procedure nano-islands expand in lateral size but become more separated from each other, leading to a narrower and stronger optical absorption spectrum. Final diameters

of the metal islands are related to evaporation rate, mass thickness, and annealing temperature and time.

In this work we fabricated Ag metal nano-island films with a height of 10 nm and varying lateral sizes of 25-75 nm as presented in the atomic force microscopy (AFM) image and scanning electron microscopy image of Figure 5.3.1 and Figure 5.3.2.

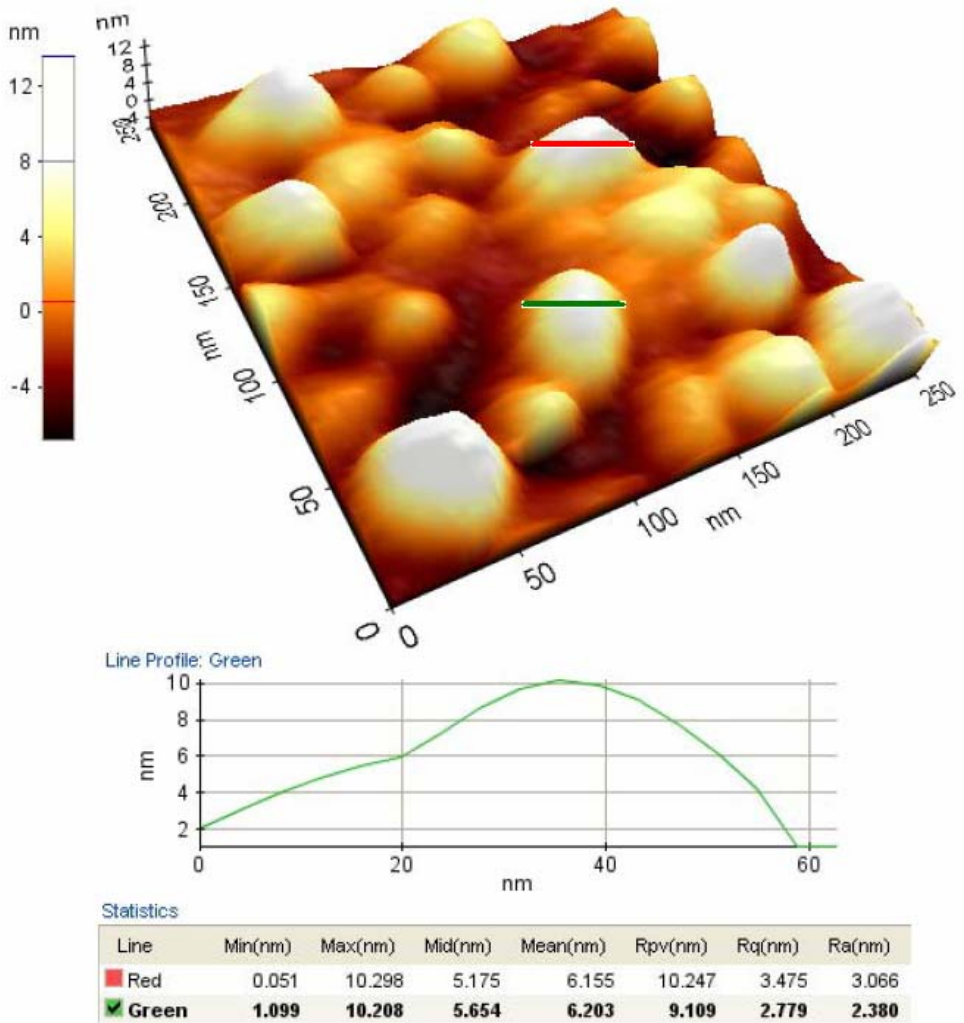

Statistics

Line	Min(nm)	Max(nm)	Mid(nm)	Mean(nm)	Rpv(nm)	Rq(nm)	Ra(nm)
Red	0.051	10.298	5.175	6.155	10.247	3.475	3.066
Green	**1.099**	**10.208**	**5.654**	**6.203**	**9.109**	**2.779**	**2.380**

Figure 5.3.1. Atomic force microscopy image of our silver nano-island film, along with dimension statistics given for green and red lines, and a line profile given for the green one.

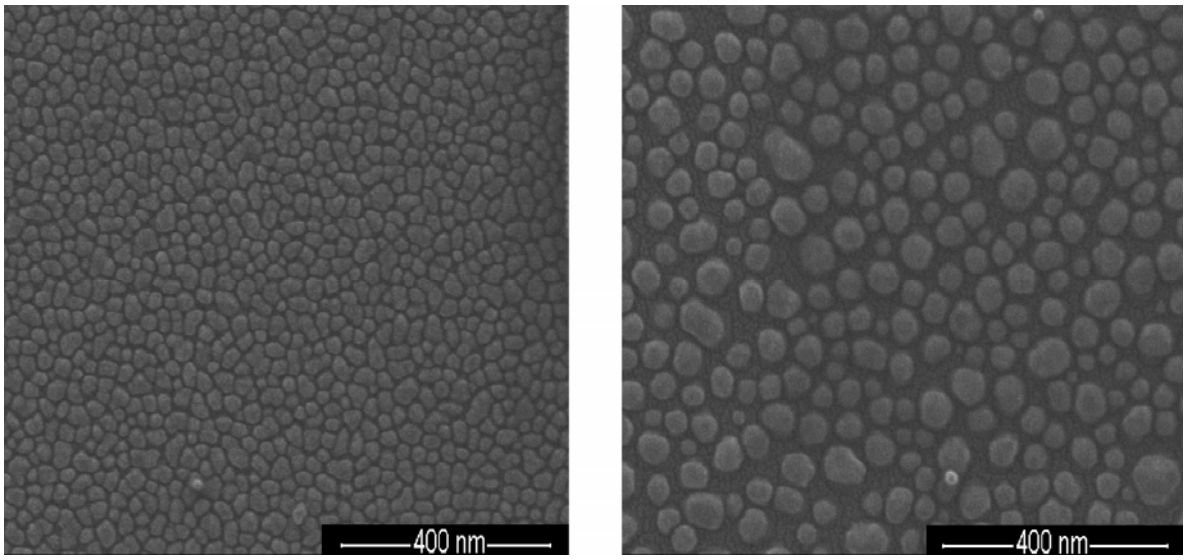

(a) (b)

Figure 5.3.2. Scanning electron microscopy image of our silver nano-island film before and after 300 ºC for 10 minutes annealing under N_2 purge.

Using these parameters we obtain localized plasmon resonance in the visible spectral region. In order to achieve the best plasmonic coupling, which necessitates a spectral overlap between the plasmonic resonance of metal nanoparticles and the surface-state emission of the NCs, we optimize all the evaporation conditions and annealing conditions for Ag.

We tune the plasmonic resonance of our Ag nano-island films by 300 ºC for 10 minutes annealing under N_2 purge, which makes them bigger as presented in Figure 5.3.2, thus resulting in a remarkable red shift of the plasmonic resonance wavelength. This annealing condition is optimal since plasmonic resonance intensity decreases due to oxidation of the Ag surface at higher temperatures, and nanoislands are not isolated enough from each other at lower temperatures.

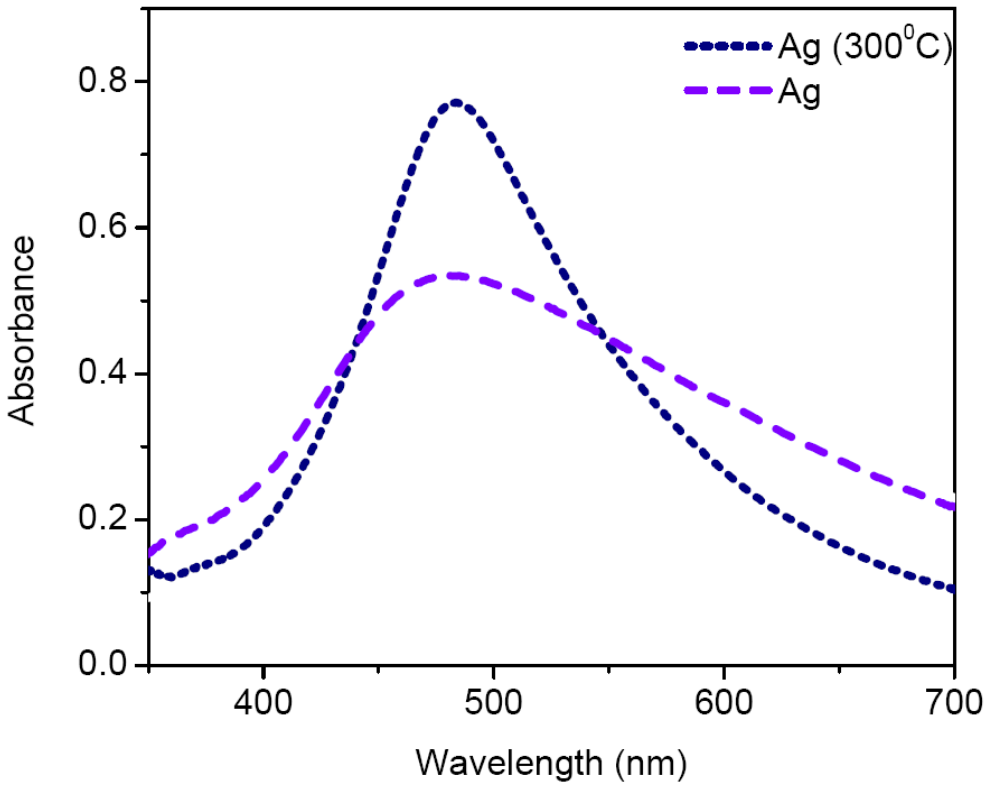

Figure 5.3.3. Optical absorption spectra of our Ag nano-islands before (dashed-purple) and after (dot-dark blue) at 300 ºC for 10 minutes annealing under N_2 purge.

Figure 5.3.3 shows the optical absorption spectra of the resulting silver nano-island films before and after annealing at 300 ºC for 10 minutes. Here, as the nano-island increases in size, we obtain a sharper but stronger optical absorption spectrum. For this work we repeated this metal nano-island formation procedure for several times and we reproducibly achieved similar results using above mentioned parameters.

5.4 Demonstration of Localized Plasmon Coupling to Trap-states of CdS Nanocrystals and Characterization Results

Nanocrystals are dissolved in a poly(methyl methacrylate) (PMMA) matrix with a concentration of 5 μM and a volume of 20 μL and spin-cast onto Ag nano-island film, which is initially deposited on quartz substrates. We also consider the presence of PMMA since the plasmon resonance peak wavelength red-shifts due to higher effective refractive index of PMMA compared to air. The amount of red shift is around 45 nm and we optimize our metal nano-island formation recipe also considering this red shift.

In our optimization process, we first study the vertical thickness by the comparison of plasmon resonance wavelength of islands corresponding to 5, 10, and 20 nm thick silver nano-island films. As depicted in Figure 5.4.1, plasmon resonance spectrum of nano-islands is strongly modified with vertical thickness change. Vertical thickness increase results in a red shift of plasmon resonance peak wavelength; also, the peak intensity decreases and the full width half maximum of the peak increases. As seen in Figure 5.4.1, after annealing, following the vertical thickness optimization procedure, we finally obtain the best spectral match between the surface-state emission of NCs and Ag nano-islands. Here spectrally the best matching nano-islands are 10 nm in vertical dimension, obtained by annealing for 300 ºC for 10 minutes with the consideration of additional NC film on top.

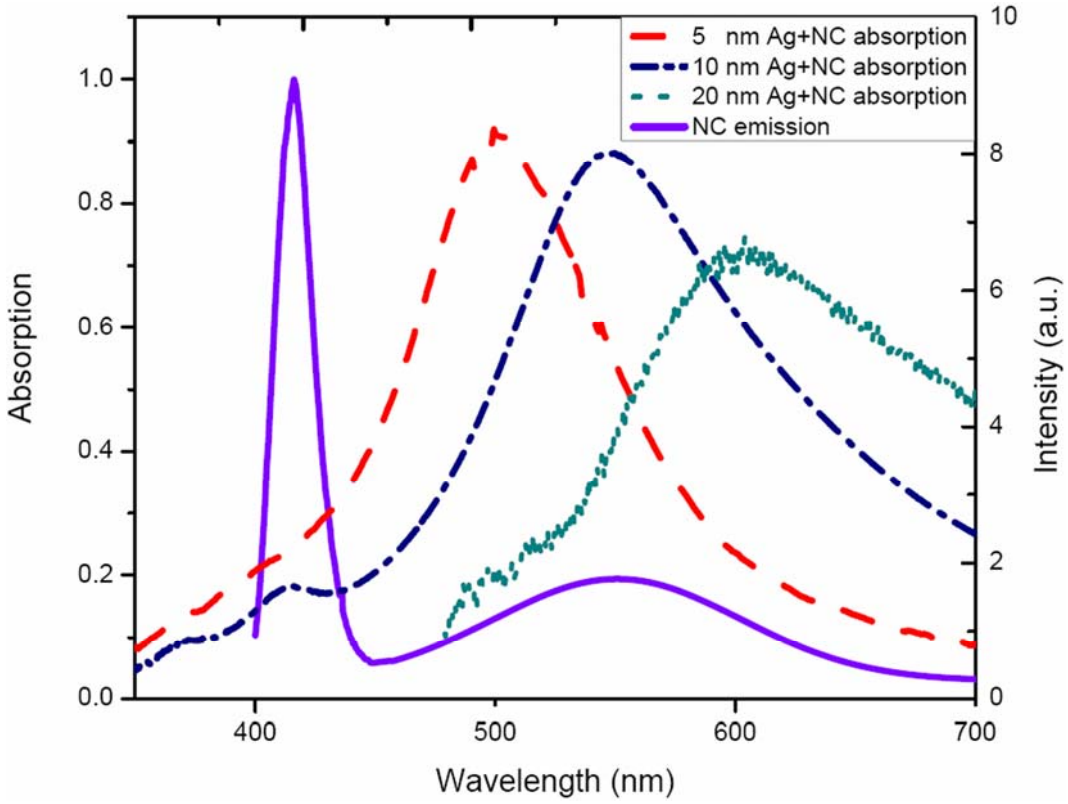

Figure 5.4.2. Optical absorption spectra of a 5 nm thick silver nano-island film with NC coating (dashed line), 10 nm thick (dash-dotted line), 20 nm thick (dotted line), and photoluminescence of trap-rich CdS NCs in PMMA (solid line).

We compare photoluminescence from plasmon coupled sample, on which 10 nm thick Ag nanoislands are coated with trap-rich 20 µl of 5 µM CdS NC on a quartz substrate, with the control group sample without Ag nanoislands. We use a He-Cd laser as an excitation source for NCs operating at 325 nm at room temperature. We use identical amounts of NCs and made the measurements under the same conditions for both samples.

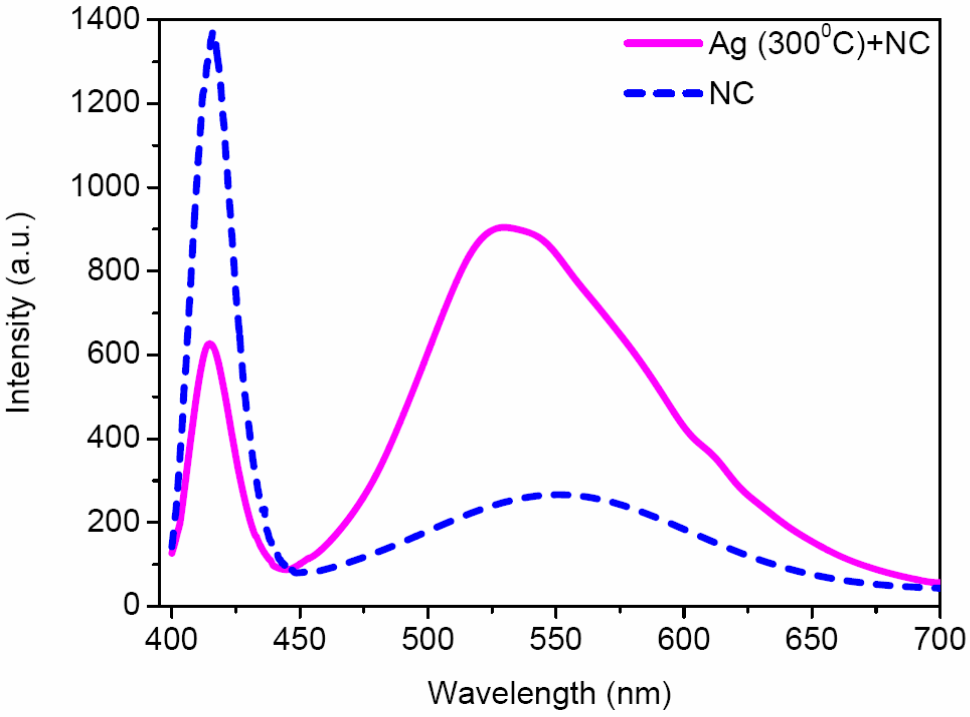

Figure 5.4.2. Photoluminescence spectra of surface-state emitting CdS NCs film alone (dotted) and when plasmon-coupled with a 10 nm thick silver nano-island film (solid).

Material on quartz substrate	Band-edge emission λ_1 (nm)	Surface-state emission λ_2 (nm)	λ_1 peak intensity (counts)	λ_2 peak intensity (counts)	Intensity ratio @λ_2 / @λ_1	Total number of photons
Only SSE NC	415	545	1388	290	0.21	67,885
SSE NC with 10 nm Ag	415	531	672	960	1.43	122,055

Table 5.4.1. Comparison of the band-edge and surface-state peak emission wavelengths, the band-edge and surface-state emission peak intensity levels, ratio of the surface-state emission to the band-edge emission, and the total number of photon counts in the emission spectrum, for the control group and the plasmon-coupled SSE NCs.

We observed significant changes in the photoluminescence spectra of the nanocrystals when they are plasmon coupled via the silver nanoisland film as

shown in Figure 5.4.2. Additionally, Table 5.4.1 presents the comparison of photoluminescence spectral values for plasmon coupled and un-coupled cases.

Plasmonic coupling decreases the band-edge emission and increases the surface-state emission of CdS NCs. When compared to no plasmon coupled case surface state emission is significantly enhanced and become dominant over the band edge emission. Surface-state emission to band edge emission peak ratio is increased by a factor of 6.8 in film and 12.7 in solution in the presence of Ag nanoislands. We also achieve an improvement in total emission from the NCs since the total number of photons emitted at all wavelengths is also enhanced by 80%. This is due to plasmon enhanced fluorescence, which affects many trap states, even though the band edge emission is suppressed.

Another important characterization for emission characteristics is the time resolved fluorescence decays of NCs. We investigate fluorescence decay curves of our samples at two different wavelengths, which correspond to emission peaks for band edge emission at 415 nm and the surface-state emission at 531 nm, both at an excitation wavelength of 284 nm. As depicted in Figure 5.4.3, the time resolved fluorescence decay curves at 415 nm shows that in the presence of plasmonic Ag nano-islands fluorescence decay is faster compared to no plasmon coupled case.

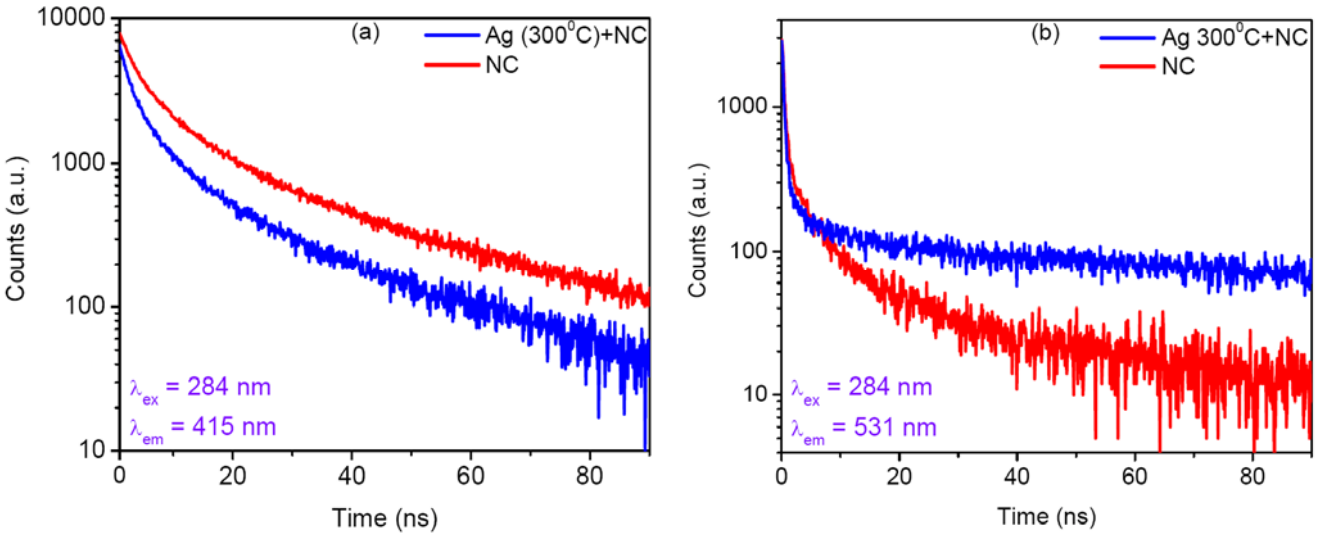

Figure 5.4.3. Time-resolved fluorescence decays of surface-state emitting CdS NCs (red) and plasmon-coupled with Ag nano-island film (blue) (a) at the band-edge emission peak wavelength of 415 nm and (b) at the surface-state emission peak wavelength of 531 nm.

At 531 nm, there is a fast component of plasmon coupled NC fluorescence decay followed by slow components compared to no plasmon coupled case. This kind of decay is hard to explain, but we can say that the presence of Ag nano-islands may lead to an increase in the energy transfer between the small NCs and bigger NCs, and this increased rate of energy transfer results in a faster decay for donor like part (415 nm) and slower decay for acceptor like part (531 nm).

In summary, we tune localized plasmon resonance wavelength by changing metal nano-island fabrication parameters and match trap-state emission wavelength of trap-rich CdS NCs to demonstrate plasmonic coupling on trap-states. We obtain a significant improvement in surface-state emission to band-edge emission ratio by a factor of 12 folds. We also achieve an overall increase of 80% in the total number of photons emitted from these white luminophor trap-rich CdS NCs. This is the first time that surface-state emission becomes dominant over the band-edge emission. We also show that plasmonic coupling is possible not only to the band-edge emission but also on the trap-state emission in a selective manner.

Chapter 6

Plasmon Coupled Förster Resonance Energy Transfer of CdTe Quantum Dots

6.1 Energy Transfer Mechanisms Effective among Nanocrystals

The Förster resonance energy transfer (FRET) is an important proximity effect, which also takes place among nanocrystals (NCs) [12]. During this phenomenon, the excitation energy of the donor nanocrystals is transferred to the acceptor nanocrystals in a non-radiative manner by the dipole-dipole coupling of the donor nanocrystal emission to the excitation of the acceptor nanocrystal. The possibility to modify energy transfer between donor and acceptor NCs is of fundamental importance for physical aspects of NC embedded photonic devices.

In addition to FRET another energy transfer mechanism of major concern is the plasmon resonance energy transfer effective among NCs and metal nanoparticles (NPs), through which the emission characteristics of excited NCs is altered via localized electric fields created by plasmonic oscillations. One favored result of this mechanism is the spontaneous emission enhancement of quantum dots in the close vicinity of metal NPs. In our approach, we combine two fundamental energy transfer mechanisms and demonstrate the plasmonic coupling of FRET between two differently sized (donor-acceptor) CdTe quantum dot nanocrystals by the use of metal nanoparticles. Steady-state and time-resolved photoluminescence properties of these plasmon coupled NCs interacting with each other via FRET are reported. We analyze consequent modifications of their emission kinetics through plasmon coupled FRET and investigate the FRET mechanism under plasmon coupling to only donor NCs and only acceptor NCs.

6.2 Experimental Demonstration of Plasmon Coupled FRET and their Optical Characterization Results

6.2.1 Layer-by-Layer Assembly Film Deposition

Using a computerized dip-coater system, we deposit monolayer films of our negatively charged Au NP, CdTe NC, PSS polymer, and positively charged PDDA polymer monolayer on our negatively charged glass substrate in a layer-by-layer (LbL) assembly. In sample preparation, Au NPs are used with as-synthesized concentrations; PDDA and PSS are used with a concentration of 2 mg/mL in 0.1 M NaCl solution. Water-soluble CdTe NC concentration is 2 mL

of 80 μM NCs in 18 mL 0.1 M NaCl solution. Dielectric spacer between donor/acceptor NCs and also metal NPs is prepared by successive deposition of positively/negatively charged PDDA/PSS polymer monolayers. This allows us to control the separation thickness at the scales of nanometers.

6.2.2 FRET Sample

As a control group we demonstrate FRET between donor NC and acceptor NC in the absence of plasmonic structures. In this structure, 1 ML of donor NC film is separated by 3 MLs of PDDA/PSS film pair from 1 ML of acceptor NC film. This structure satisfies the Förster radius range for FRET mechanism, regarding the dielectric spacer and surfactants/ligands between NCs. Figure 6.2.2.1 presents the donor NC emission spectrum and the acceptor NC absorption spectrum. Here we observe a strong spectral overlap between the absorption of acceptor NC and the emission of donor NC, which also needs to be satisfied for FRET condition.

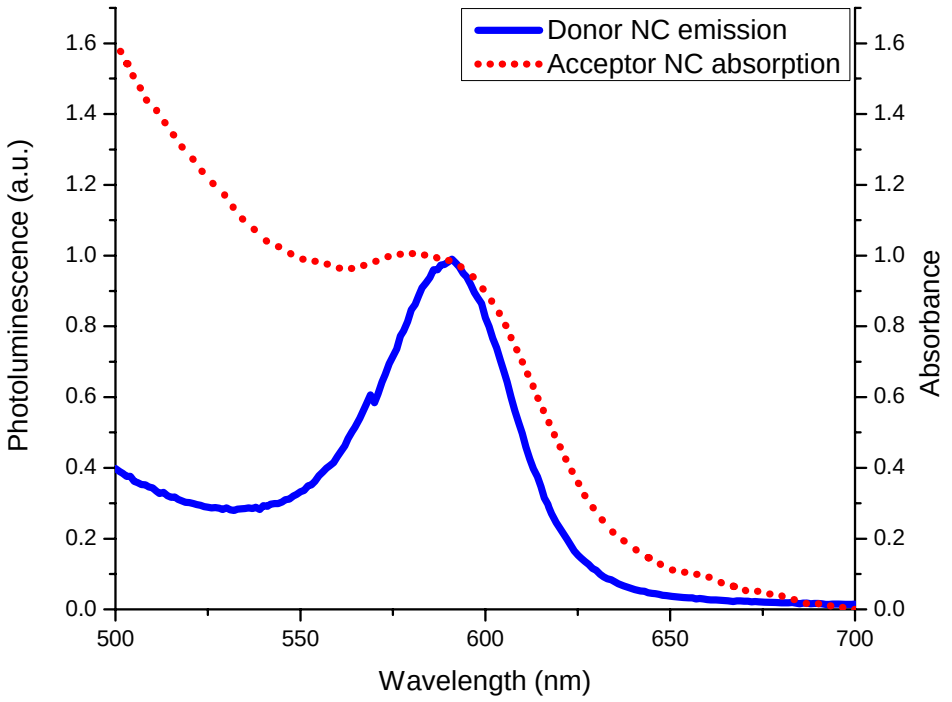

Figure 6.2.2.1. Photoluminescence spectrum of donor CdTe NCs given with the optical absorption spectrum of acceptor CdTe NCs.

In FRET sample, the acceptor emission is enhanced while the donor emission is suppressed simultaneously as depicted in Figure 6.2.2.2. We observe a 1.43-fold emission enhancement of the acceptor NCs due to FRET. Additionally, the amplitude averaged photoluminescence lifetimes of the donor NCs decreases from 1.33 to 0.87 ns, while the lifetime of the acceptor NCs increases from 1.53 to 3.11 ns (as later shown in Figure 6.2.3.3 and Figure 6.2.3.4). These photoluminescence decay lifetime modifications provide evidence for strong energy transfer between these donor and acceptor NCs.

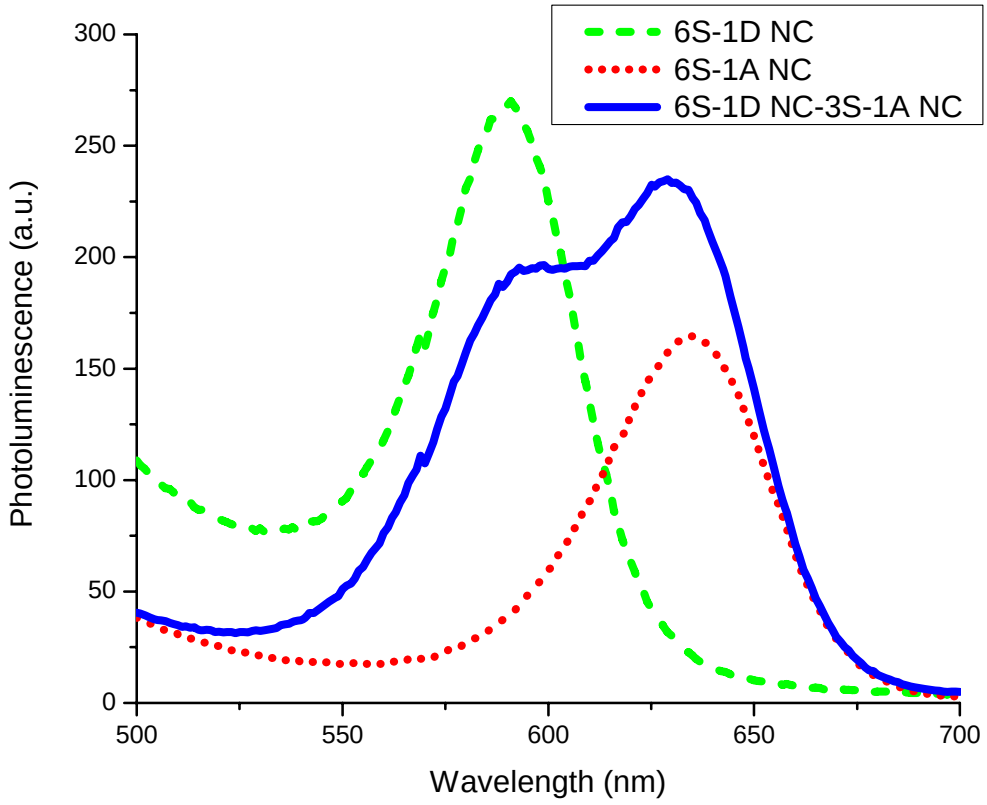

Figure 6.2.2.2. Photoluminescence spectra of donor NCs, acceptor NCs, and donor and acceptor NCs under FRET condition.

We fit our photoluminescence decay curves using a tri-exponential decay fit (Fluo-fit decay fit program of PicoQuant Technologies). Using the time-resolved fluorescence decay fit parameters we calculate FRET rates between the donor and acceptor NCs. Using these decay rates we also compute the FRET efficiency of the prepared samples. For our first system described here, we calculate the energy transfer rate to be 0.39 ns^{-1}. Also we find out the FRET efficiency to be 0.35.

6.2.3 FRET Sample with Plasmon Coupling to Acceptor NCs

As described in the previous chapter, in order to obtain plasmon enhanced NC emission the separation between NC layer and metal NP layers should be optimized. In the case of short distance between semiconductor NCs and metal NPs, the emission is quenched due to non-radiative energy transfer between these species. Also, in the case of a long distance between NCs and metal NPs the localized electric field generated by metal NPs vanishes and does not modify the photoluminescence mechanisms of NCs. The enhanced emission occurs in a very narrow range of separation distance, which is approximately 5-20 nm (including surfactants and ligands). Our spacer optimization results show that the strongest emission enhancement is observed in the presence of 6 ML PDDA and PSS pairs in successive deposition. In our plasmon coupled FRET sample, following the Au NPs and PDDA/PSS spacer layers, we deposit 1 ML of CdTe NC, which serves as the acceptor (A) species in FRET mechanism. We used only a single monolayer of NC in our experiments because there is also additional energy transfer between each monolayer in the presence of a few NC layers and also the separation between metal NPs and each NC layer in the structure is different, which complicates the understanding of photo-physical emission mechanisms. But, a significant drawback of the use of a single NC layer is very low emission/absorption signals, which makes their experimental characterizations (photoluminescence, absorption, and time-resolved fluorescence decay) much more difficult. We overcome this issue, by synthesizing CdTe NCs with very high quantum efficiencies and optimized the use of setups (e.g. fluorometer, spectrophotometer) by integrating a new setup tools inside.

In this part, only the acceptor NCs are plasmon-coupled using Au NPs. There are 6 ML of Au NPs separated by 6 ML of PDDA/PSS pair followed by 1 ML

of acceptor NCs. Figure 6.2.3.1 presents the photoluminescence spectra of the acceptor NCs alone and in the presence of Au NPs. Here we observe that the emission of NC film layer is increased by a factor of 2.81 under strong plasmon coupling.

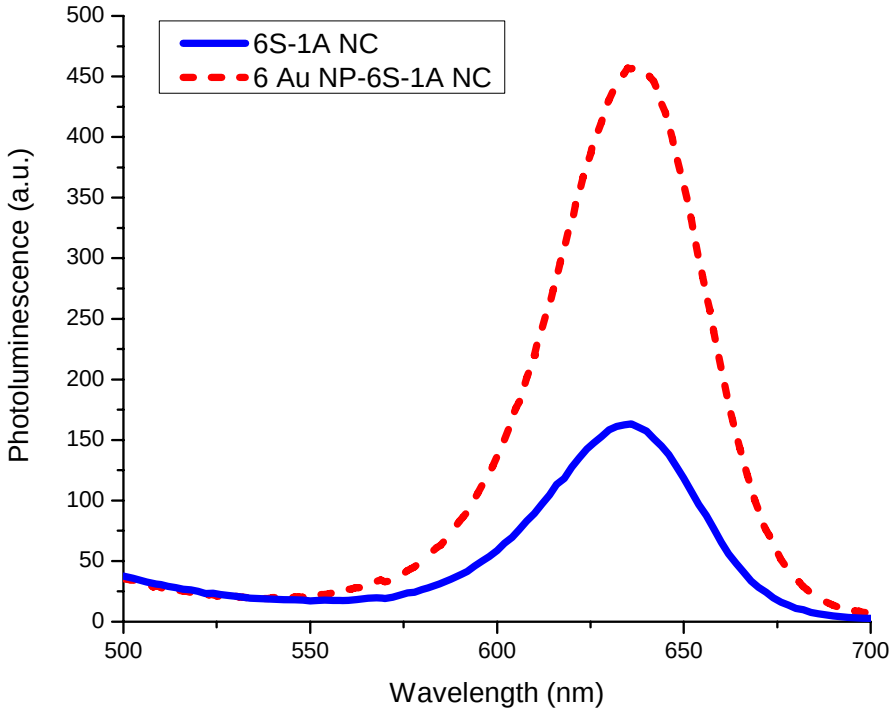

Figure 6.2.3.1. Photoluminescence spectra of acceptor CdTe NCs alone, and in the presence of Au NPs.

Subsequently we repeat the same FRET experiment by the use of plasmon coupled acceptor NC film layer. Plasmon coupled acceptor NC is separated by 3 ML of PDDA/PSS pairs and finally 1 ML of donor NC layer is deposited. As depicted in Figure 6.4, there is a significant increase in the emission level of acceptor NC layer. Due to long separation distance, donor NCs are not influenced by the plasmonic resonance of Au NPs. Then we can say that mechanisms that increase acceptor emission are the combination of both FRET between donor and acceptor NCs and plasmon coupling to acceptor NC layer. Here we observe 2.86 folds emission enhancement of the acceptor NC.

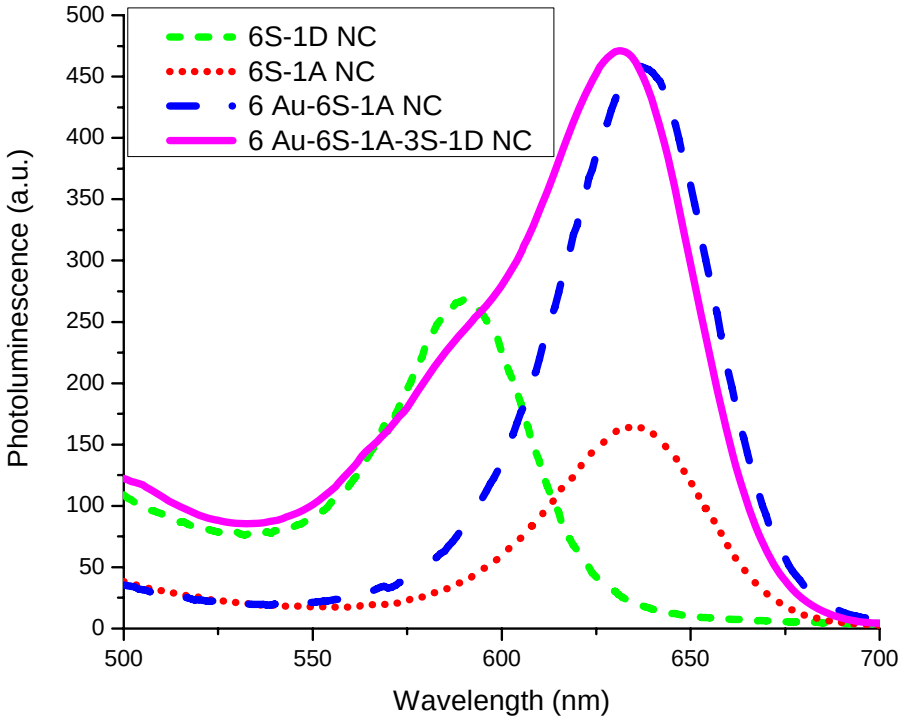

Figure 6.2.3.2. Photoluminescence spectra of only donor NCs, only acceptor NCs, acceptor NCs in the presence of metal NPs (dashed), and donor and acceptor NCs under FRET condition in the presence of metal NPs plasmon coupled to acceptor NCs.

Further investigations of PL mechanisms through the time-resolved photoluminescence decay lifetimes of NC layers are depicted in Figure 6.2.3.3. Since plasmons coupled to the acceptor NCs, the donor NCs lifetime is not considerably modified and is found to be 1.31 ns, being very close to its initial value (1.33 ns). Finally, in the presence of Au NPs coupled to acceptor NCs, we observe a reduction in the lifetime of donor to 0.89 ns, which is very close to the lifetime value of donor NCs in the presence of acceptor NCs and in the absence of Au NPs (0.87 ns). The lifetime reductions are mostly due to FRET between the donor and acceptor NCs.

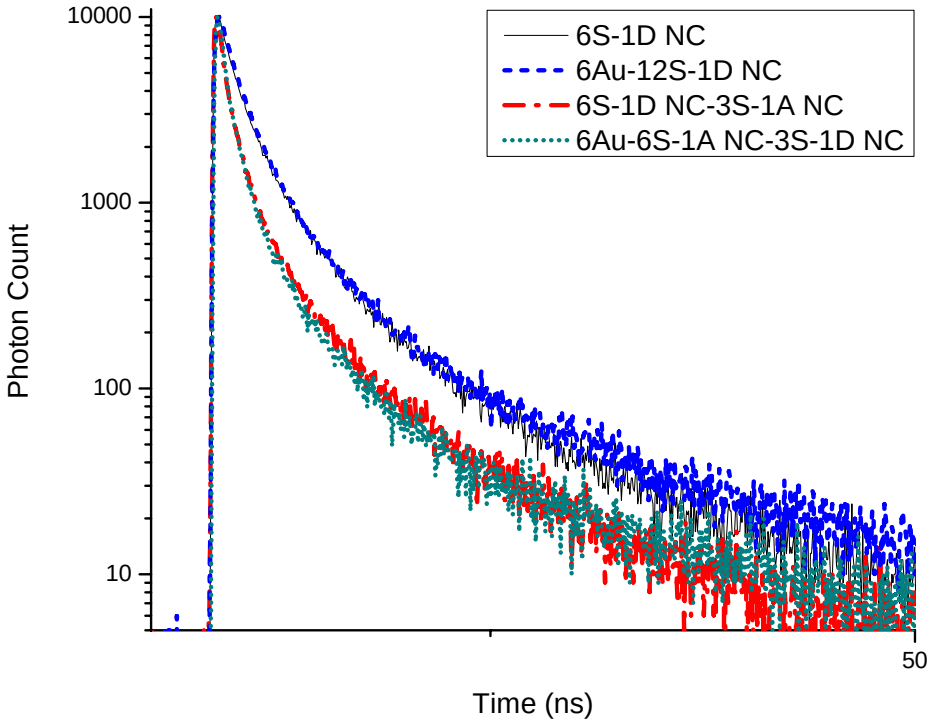

Figure 6.2.3.3. Time-resolved fluorescence decays of CdTe NCs at the donor NCs emission peak wavelength, also in the presence of metal NPs, acceptor NCs, and both.

At the acceptor NC emission wavelength, in the presence of Au NPs coupled to acceptor NCs, the acceptor photon decay lifetime decreases from 1.53 ns to 0.97 ns as depicted in Figure 6.2.3.4. Then in the presence of Au NPs (coupled to acceptor NCs only) and donor NCs, we observe an increase in the lifetime of acceptor NCs from 1.53 ns to 1.91 ns. Even though there is a strong FRET mechanism taking place between the donor and acceptor NCs, the amplitude averaged lifetime of the acceptor NCs is not increased as in the previous sample since plasmonic coupling decreases the lifetimes of NCs.

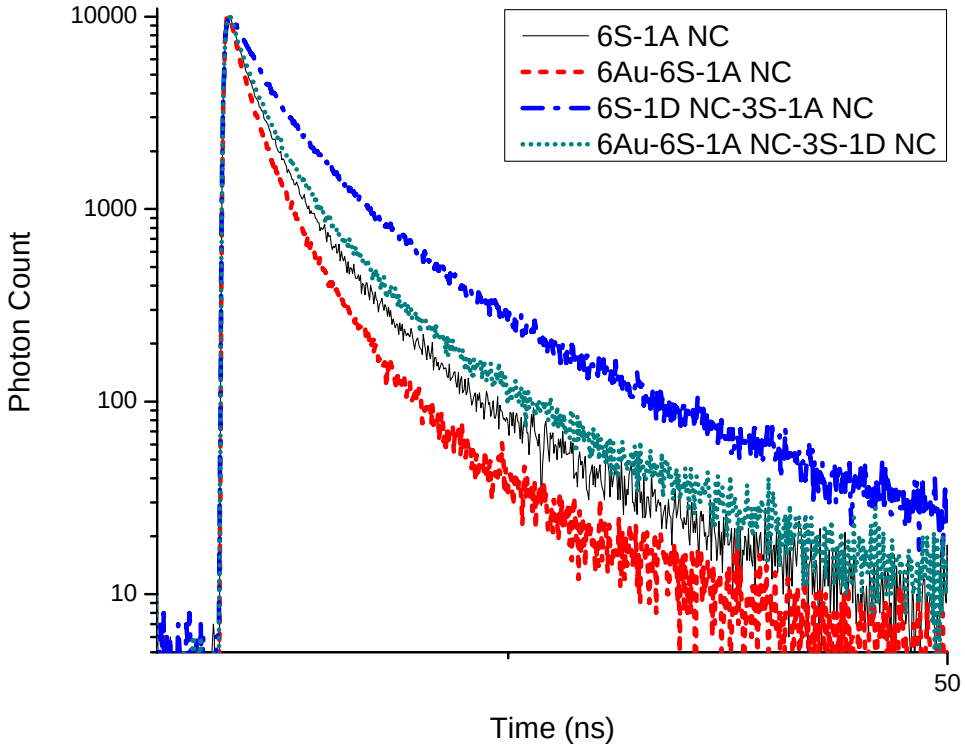

Figure 6.2.3.4. Time-resolved fluorescence decays of CdTe NCs at the acceptor NCs emission peak wavelength, also in the presence of metal NPs, donor NCs, and both.

For the system described above, we calculate the energy transfer rate to be 0.37 ns^{-1}.

6.2.4 FRET Sample with Plasmon Coupling to Donor NCs

We deposit 6 ML films of Au NPs to obtain a strong plasmonic resonance as presented in Figure 6.2.4.1 Plasmon resonance spectrum spans a wide range of visible wavelengths and match donor and acceptor NCs emission spectra.

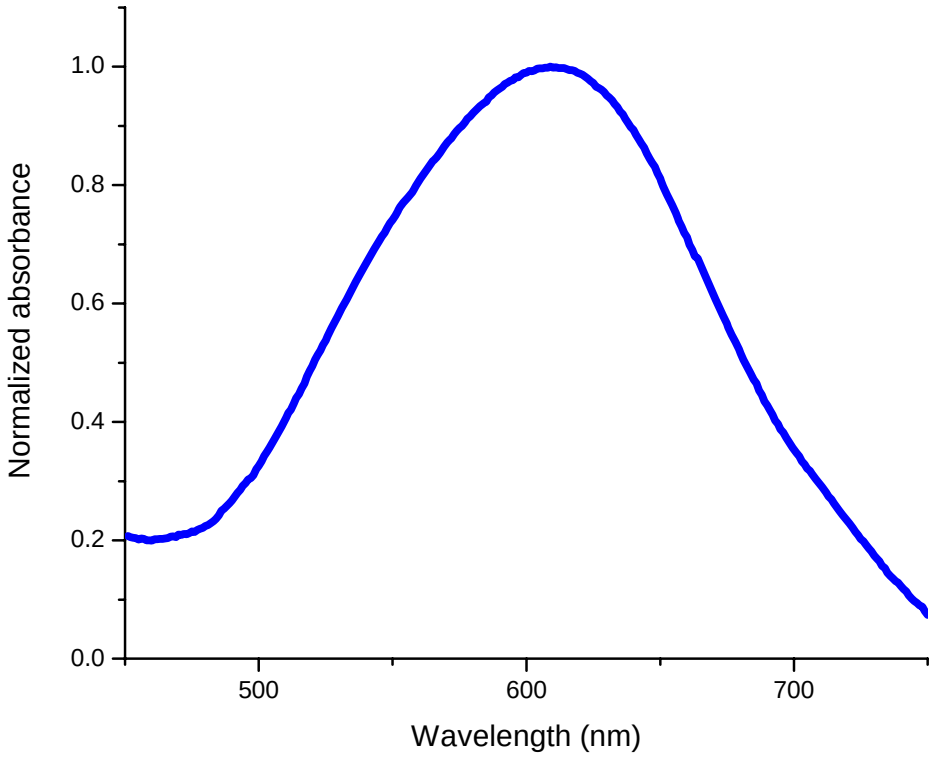

Figure 6.2.4.1. Normalized optical absorption spectrum of 6 monolayer Au NPs deposited on a glass substrate.

Using optimized recipe for metal enhanced fluorescence we observe that donor NC emission is increased by a factor of 2.23 in the presence of metal NPs due to plasmon coupling as depicted in Figure 6.2.4.2.

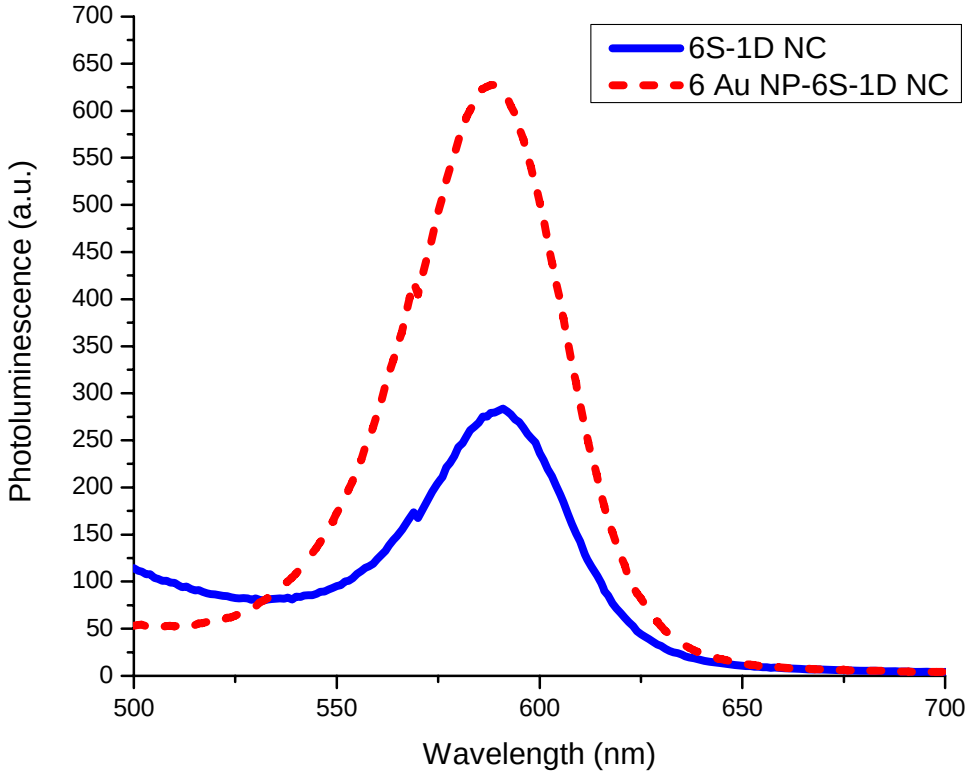

Figure 6.2.4.2. Photoluminescence spectra of our CdTe NCs alone, and in the presence of metal NPs.

Subsequently we repeat FRET experiment by the use of plasmon coupled donor NCs. Plasmon coupled donor NC layer is separated by 3 ML of PDDA/PSS pairs and finally 1 ML of acceptor NC film layer is deposited. As depicted in Figure 6.2.4.3, there is a significant increase in the emission levels of both donor and acceptor NCs. According to our experiments acceptor NCs are not influenced by the plasmonic resonance of the Au NPs due to long separation distance. The effective mechanism on emission is the enhanced FRET due to significant increase in excitation and emission levels of donor NC in the presence of Au NPs. Here we observe a 2.26-fold emission enhancement of the acceptor NC. This emission enhancement is higher compared to only FRET mechanism with a 1.43-fold enhancement.

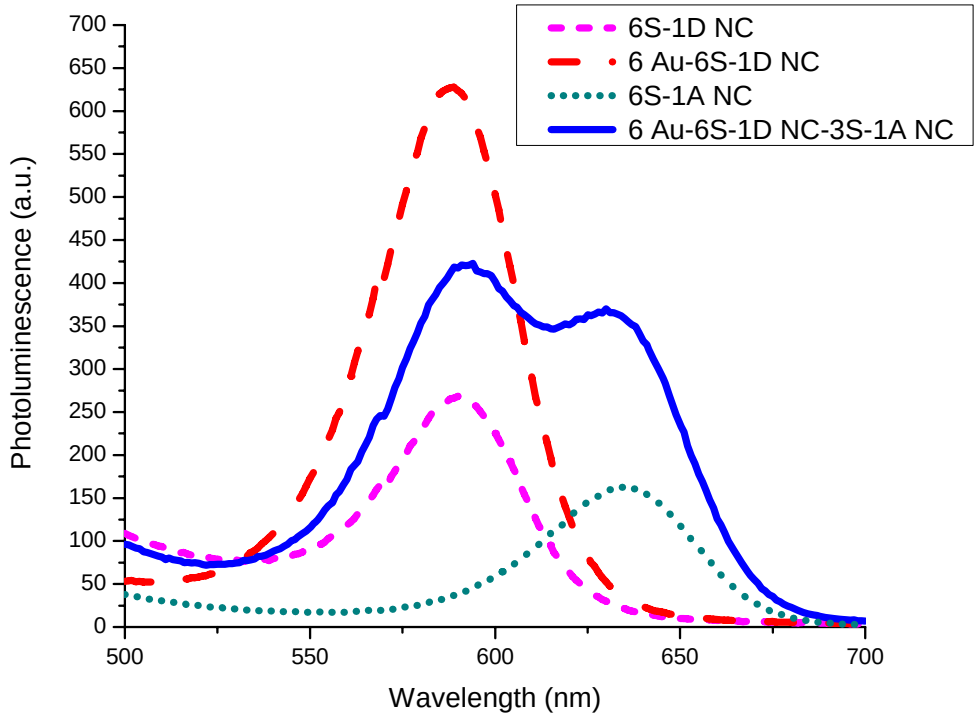

Figure 6.2.4.3. Photoluminescence spectra of donor NCs, acceptor NCs, donor NCs in the presence of metal NPs (dashed), and donor and acceptor NCs in FRET condition in the presence of metal NPs plasmon coupled to donor NCs.

We further investigate modified PL mechanisms through the time-resolved photoluminescence decay lifetimes of NC layers as shown in Figure 6.2.4.4. At the donor emission wavelength, donor NCs have an amplitude averaged decay lifetime of 1.33 ns. In the presence of Au NPs, donor NCs lifetime decreases down to 0.43 ns due to plasmon resonance energy transfer. In the presence of acceptors, donor NCs lifetime decreases to 0.87 ns due to FRET between the donor and acceptor NCs. Finally in the presence of Au NPs (coupled to donor NCs only) and acceptor NCs, we observe a significant reduction in the lifetime of donor NCs from 1.33 ns to 0.25 ns showing a strong energy transfer between all species.

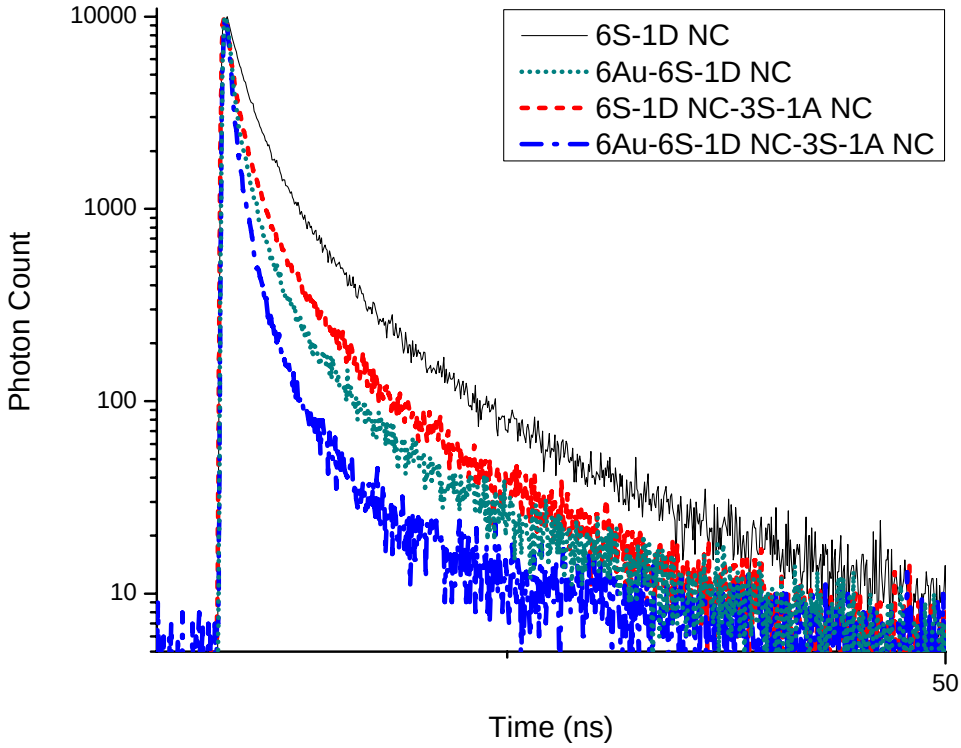

Figure 6.2.4.4. Time-resolved fluorescence decays of CdTe NCs at the donor NCs emission peak wavelength, also in the presence of metal NPs, donor NCs, and both.

At the acceptor NC emission wavelength, the acceptor NCs have an amplitude averaged decay lifetime of 1.53 ns as depicted in Figure 6.2.4.5. In the presence of Au NPs coupled to donor NCs, acceptor NCs is not directly influenced and their lifetime slightly decreases to 1.44 ns. In the presence of donors, acceptor NCs lifetime increases to 3.11 ns due to FRET between the donor and acceptor NCs. Finally in the presence of Au NPs (coupled to donor NCs only) and donor NCs, we observe a significant increase in the lifetime of acceptor NCs from 1.53 ns to 3.91 ns showing a strong energy transfer.

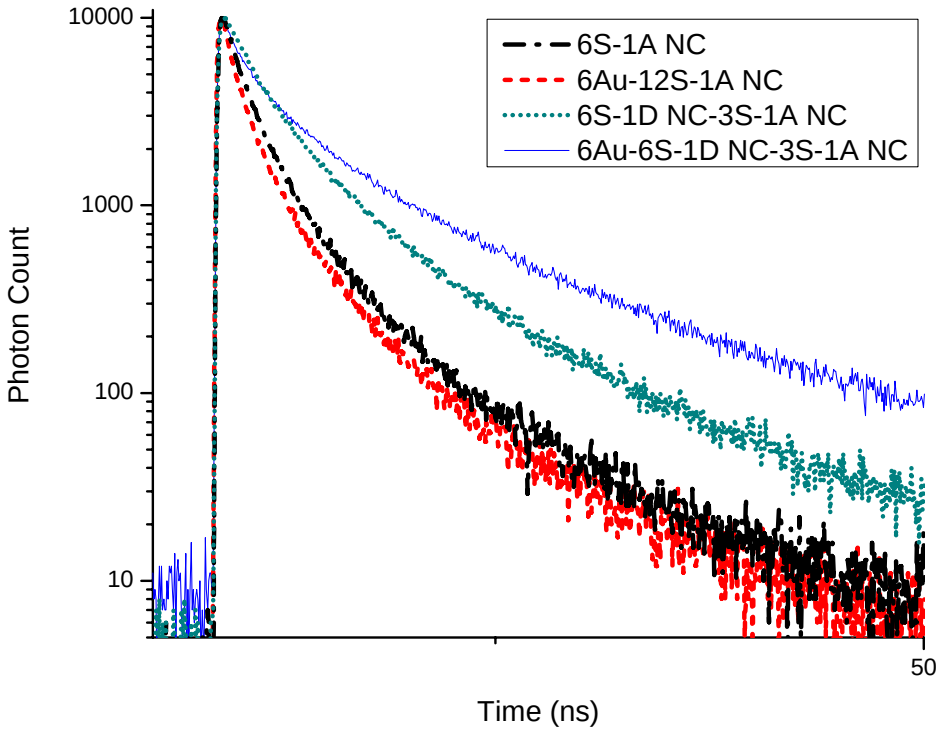

Figure 6.2.4.5. Time-resolved fluorescence decays of CdTe NCs at the acceptor NCs emission peak wavelength, also in the presence of metal NPs, donor NCs, and both.

For the system described above, we calculate the energy transfer rate to be 0.49 ns^{-1}.

In this work, we conclude that plasmon coupling enhances non-radiative energy transfer. This plasmon coupled FRET is observed both for the cases when the acceptor of the FRET pair is plasmon-coupled as well as when the donor of the FRET pair is plasmon-coupled. In both cases, the enhancement in the acceptor emission with plasmon coupling is significantly larger in FRET than that with no plasmon coupling.

Chapter 7

Conclusion

In this thesis we worked on the understanding and development of highly efficient emitters/absorbers using two different energy transfer mechanisms; resonance energy transfer between metal nanoparticles and nanocrystals, and Förster resonance energy transfer between two differently sized nanocrystals. We introduced the fundamentals of surface plasmons and explained the effective parameters on the surface plasmon resonance frequency. We also introduced nanocrystals including their theoretical aspects, colloidal synthesis and optical characterizations.

In the following chapters we presented our experimental details and characterization results. First, we used a layer-by layer film deposition method to coat CdTe nanocrystal layers and Au nanoparticles on glass substrates. We studied the optimization of unit cell structures including metal NP and semiconductor NC films separated by dielectric PDDA/PSS polymer bilayers. We observed that repetitive deposition of an optimized unit cell structure results in the enhancement of NC emission. In the 5 times repeating unit cell structure of Au and CdTe nanocomposite film separated by dielectric layer, we demonstrated a significant enhancement of CdTe NC emission by a factor of 4.37, where the quantum efficiency is enhanced to reach a high level of 30% in film.

We also tuned localized plasmon resonance wavelength by changing metal nano-island fabrication parameters and matched trap-state emission wavelength of trap-rich CdS NCs to demonstrate plasmonic coupling on trap-states. We obtained a significant improvement in the surface-state emission to band-edge emission ratio by a factor 12. We also achieved an overall increase of 80% in the total number of photons emitted from these white luminophor trap-rich CdS NCs. This is the first time that surface-state emission dominates over the band-edge emission. This work shows that it is possible to plasmon couple not only to the band-edge emission but also to trap-state emission in a selective manner.

Additionally, we reported on the steady-state and time-resolved photoluminescence properties of these plasmon-coupled NCs interacting with each other via FRET and analyze consequent modifications of their emission kinetics through plasmon coupled FRET. We investigated the FRET mechanism under the plasmon coupling to only donor NCs and only acceptor NCs.

During this thesis work, we published an SCI paper from Chapter 5 as given in the reference [62]. We are also in the submission process of Chapter 4 and Chapter 6 to SCI journals. Moreover, Chapter 4 [63] and Chapter 5 [64] materials are accepted for refereed international conference presentations. We also submitted Chapter 6 material to a refereed international conference [65].

BIBLIOGRAPHY

[1] D. Harden, *Glass of the Caesars*, exh. cat. London, The British Museum Press 1988.

[2] M. Faraday, "Experimental Relations of Gold (and Other Metals) to Light," *Philos. Trans. R. Soc. London*, vol. 147, 1857, pp. 145.

[3] G. Mie, "Considerations on the optic of turbid media, especially colloidal metal sols," *Ann. Phys.*, vol. 25, 1908, pp. 377-442.

[4] C. D. Geddes and J. R. Lakowicz, "Metal-enhanced fluorescence", *J. Fluoresc.*, vol. 12, 2002, pp. 121-129.

[5] A. Otto, I. Mrozek, H. Grabborn and W. Akemann, "Surface-enhanced Raman scattering," *J. Phys.: Condens. Matter*, vol. 4, 1992, pp. 1143-1212.

[6] T. Y. F. Tsang, "Surface-plasmon-enhanced third-harmonic generation in thin silver films," *Opt. Lett.*, vol. 21, 1996, pp. 245-247.

[7] H. Kano and S. Kawata, "Two-photon-excited fluorescence enhanced by a surface plasmon," *Opt. Lett.,* vol. 21, no. 22, 1996, pp. 1848-1850.

[8] S. Nizamoglu, T. Ozel, E. Sari and H. V. Demir, "White light generation using CdSe/ZnS core-shell nanocrystals hybridized with InGaN/GaN light emitting diodes," *Nanotechnology*, vol. 18, 2007, 065709.

[9] E. Mutlugun, I. M Soganci, and H. V. Demir, "Photovoltaic nanocrystal scintillators hybridized on Si solar cells for enhanced conversion efficiency in UV," *Opt. Express,* vol. 16, 2008, pp. 3537-3545.

[10] D. Alexson, H. Chen, M. Cho, M. Dutta, Y. Li, P. Shi, A. Raichura, D. Ramadurai, S. Parikh, M. A. Stroscio and M. Vasudev, "Semiconductor nanostructures in biological applications," *J. Phys. : Condens. Matter.*, vol. 17, 2005, pp. 637-656.

[11] A. A. Chistyakov, I. L. Martynov, K. E. Mochalov, V. A. Oleinikov, S. V. Sizova, E. A. Ustinovich, and K. V. Zakharchenko, "Interaction of CdSe/ZnS core-shell semiconductor nanocrystals in solid thin films," *Laser Phys.,* vol. 16, 2006, pp. 1625-1632.

[12] J. R. Lakowicz, *Principles of Fluorescence Spectroscopy*, Plenum Publishing Corporation, 2nd edition, 1999.

[13] O. Kulakovich, N. Strekal, A. Yaroshevich, S. Maskevich, S. Gaponenko, I. Nabiev, U. Woggon and M. Artemyev, "Enhanced Luminescence of CdSe Quantum Dots on Gold Colloids," *Nano Lett.*, vol. 2, 2002, pp. 1449-1452.

[14] a) M. Futamata, Y. Maruyama and M. Ishikawa, "Local Electric Field and Scattering Cross Section of Ag Nanoparticles under Surface Plasmon Resonance by Finite Difference Time Domain Method," I, vol. 107, 2003, pp. 7607-7617; b) T. Nakamura and S. Hayashi, "Enhancement of Dye Fluorescence by Gold Nanoparticles: Analysis of Particle Size Dependence," *Jpn. J. Appl. Phys.*, vol. 44, 2005, pp. 6833-6837.

[15] a) Y. Fedutik, V. Temnov, O. Schöps, U. Woggon and M. V. Artemyev, "Exciton−Plasmon Interaction in a Composite Metal-Insulator-Semiconductor Nanowire System," *JACS*, vol. 129, 2007, pp. 14939-14945; b) Y. Fedutik, V. Temnov, O. Schöps, U. Woggon and M. V. Artemyev, "Exciton-Plasmon-Photon Conversion in Plasmonic Nanostructures," *Phys. Rev. Lett.*, vol. 99, 2007, 136802.

[16] I. M. Soganci, S. Nizamoglu, E. Mutlugun, O. Akin and H. V. Demir, "Nanocrystal hybridized scintillators for enhanced detection and imaging on Si platforms in UV," Opt. Express, vol. 15, 2007, pp. 1128-1134.

[17] T. Förster, "Zwischenmolekulare Energiewanderung und Fluoreszenz," *Ann. Physik,* vol. 437, 1948, pp. 55-75.

[18] V. M. Agranovich and D. L. Mills, *Surface Polaritons: Electromagnetic Waves at Surfaces and Interfaces*, North-Holland, Amsterdam, 1992.

[19] S. Kawata (Ed.), *Near-Field Optics and Surface Plasmon Polaritons*, Springer Verlag, Berlin, 2001.

[20] K. Sönnichsen, *Plasmons in Metal Nanostructures*, Ludwig-Maximilians University of Munich, 2001.

[21] K. L. Kelly, E. Coronado, L. L. Zhao and G. C. Schatz, "The optical properties of metal nanoparticles: the influence of size, shape, and dielectric environment," *J. Phys. Chem. B*, vol. 107, 2003, pp. 668-677.

[22] U. Kreibig and M. Vollmer, *Optical Properties of Metal Clusters*, Springer Verlag, Berlin, 1995.

[23] L. M. Liz-Marzan, "Tailoring surface plasmons through the morphology and assembly of metal nanoparticles," *Langmuir,* vol. 22, 2006, pp. 32-41.

[24] J. R. Heath, C. M. Knobler and D. V. Leff, "Pressure/temperature phase diagrams and superlattices of organically functionalized metal nanocrystal monolayers: The influence of particle size, size distribution, and surface passivant," *J. Phys. Chem. B*, vol. 101, 1997, pp. 189-197.

[25] S. W. Chen, R. S. Ingram, M. J. Hostetler, J. J. Pietron, R. W. Murray, T. G. Schaaff, J. T. Khoury, M. M. Alvarez and R. L. Whetten, "Gold nanoelectrodes of varied size: Transition to molecule-like charging," *Science*, vol. 280, 1998, pp. 2098-2101.

[26] M. M. Alvarez, J. T. Khoury, T. G. Schaaff, M. N. Shafigullin, I. Vezmar and R. L. Whetten, "Optical absorption spectra of Nanocrystal Gold molecules," *J. of Phys. Chem. B*, vol. 101, 1997, pp. 3706-3712.

[27] M. A. El-Sayed, "Some interesting properties of metals confined in time and nanometer space of different shapes," *Acc. of Chem. Research*, vol. 34, 2001, pp. 257-264.

[28] R. C. Jin, Y. W. Cao, C. A. Mirkin, K. L. Kelly, G. C. Schatz and J. G. Zheng, "Photoinduced conversion of silver nanospheres to nanoprisms," *Science*, vol. 294, 2001, pp. 1901-1903.

[29] A. Henglein, "Electronics of colloidal nanometer particles," *Berichte Der Bunsen-Gesellschaft-Phys. Chem. Chem. Phys.*, vol. 99, 1995, pp. 903-913.

[30] B. Rodriguez-Gonzalez, A. Burrows, M. Watanabe, C. J. Kiely and L. M. Marzan, "Multishell bimetallic AuAg nanoparticles: synthesis, structure and optical properties," *J. Mat. Chem.*, vol. 15, 2005, pp. 1755-1759.

[31] P. Mulvaney, M. Giersig and A. Henglein, "Electrochemistry of multilayer colloids: preparation and absorption spectrum of gold-coated silver particles," *J. Phys. Chem.*, vol. 97, 1993, pp. 7061-7064.

[32] L.M. Liz-Marzán, M. Giersig and P. Mulvaney, "Synthesis of nanosized gold-silica core-shell particles," *J. Phys. Chem*, vol. 12, 1996, pp. 4329-4335.

[33] P. Drude, "Zur Elektronentheorie der metalle," *Annalen der Physik*, vol. 306, 1900, p. 566-613.

[34] P. Mulvaney, "Surface plasmon spectroscopy of nanosized metal particles," *Langmuir*, vol. 12, 1996, pp. 788-800.

[35] T. Hirakawa and P. V. Kamat, "Charge separation and catalytic activity of Ag@TiO2 core-shell composite clusters under UV-irradiation," *JACS*, vol. 127, 2005, pp. 3928-3934.

[36] Z. S. Pillai and P. V. Kamat, "What factors control the size and shape of silver nanoparticles in the citrate ion reduction method?," *J. Phys. Chem. B*, vol. 108, 2004, pp. 945-951.

[37] G. D. Sockalingum, A. Beljebbar, H. Morjani, J. F. Angiboust and M. Manfait, "Characterization of island films as surface-enhanced Raman spectroscopy substrates for detecting low antitumor drug concentrations at single cell level", *Biospectroscopy*, vol. 4, 1998, pp. 71-78.

[38] M. Westphalen, U. Kreibig, J. Rostalski, H. Luth and D. Meissner, "Metal cluster enhanced organic solar cells," *Solar Energy Materials & Solar Cells*, vol. 61, 2000, pp. 97-105.

[39] H. Fröhlich, *Physica* , vol. 4,1937, pp. 406−412.

[40] A. Ekimov, "Exciton light absorption by CuCl micro crystals in glass matrix," *Sov. Glass Phys. Chem.*, vol.6, 1980, pp. 511-512.

[41] R. Rossetti, R., et al. "Quantum size effect in the redox potential, resonance Raman spectra, and electronic spectra of CdS crytallites in aqueous solution," *J. Chem. Phys.*, vol. 79, 1983, pp. 1086-1088.

[42] H. Tong and Y.J. Zhu , "Synthesis of CdS nanocrystals based on low-temperature thermolysis of one single-source organometallic precursor, " *Nanotechnology*, vol. 17, 2006, pp. 845-851.

[43] A. L. Rogach, A. Kornowski, M. Gao, A. Eychmu1ller and H. Weller "Synthesis and Characterization of a Size Series of Extremely Small Thiol-Stabilized CdSe Nanocrystals," *J. Phys. Chem. B*, vol. 103, 1999, pp. 3065-3069.

[44] M.Gao, S. Kirstein, H. Möhwald, A. L. Rogach, A. Kornowski, A. Eychmüller and H. Weller, "Strongly Photoluminescent CdTe Nanocrystals by Proper Surface Modification," *Phys. Chem. B*, vol. 102, 1998, pp. 8360-8363.

[45] R. N. Bhargava, D. Gallagher, X. Hong and A. Nurmikko, "Optical Properties of Manganese-Doped Nanocrystals of ZnS," *Phys. Rev. Lett.*, vol.72, 1994, pp. 416-419.

[46] M. A. Hines and G.D. Scholes, "Colloidal PbS nanocrystals with size-tunable near-infrared emission: Observation of post-synthesis self-narrowing of the particle size distribution," *Adv. Mater.*, vol. 15, 2003, pp. 1844-1849.

[47] B. Delley and E.F. Steigmeier, "Quantum confinement in Si nanocrystals," *Phys. Review B*, vol. 47, 1993, pp. 1397-1400.

[48] S. Okamoto and Y. Kanemitsu, "Photoluminescence properties of surface-oxidized Ge nanocrystals: Surface localization of excitons," *Phys. Rev. B*, vol. 54, 1996, pp. 16422-16424.

[49] D. V. Talapin, A. L. Rogach, A. Kornowski, M. Haase and H.Weller "Highly Luminescent Monodisperse CdSe and CdSe/ZnS Nanocrystals Synthesized in a Hexadecylamine-Trioctylphosphine Oxide-Trioctylphospine Mixture," *Nano Lett.*, vol. 1, 2001, pp. 207-211.

[50] S. Kim, B. Fisher, H-J. Eisler and M. Bawendi, "Type-II Quantum Dots: CdTe/CdSe(Core/Shell) and CdSe/ZnTe(Core/Shell) Heterostructures," *JACS*, vol. 125, 2003, pp. 11466 -11467.

[51] http://www.evidenttech.com/quantum-dots-explained/how-quantum-dots-work

[52] S. V. Gaponenko, *Optical Properties of Semiconductor Nanocrystals*, Cambridge University Press, Cambridge, 1998.

[53] H.-J. Eisler, V. C. Sundar, M. G. Bawendi, M. Walsh, H. I. Smith and V. Klimov, "Color-selective semiconductor nanocrystal laser," *Appl. Phys. Lett.*, vol. 80, 2002, pp. 4614-4616.

[54] M. B. Fischbein and M. Drndic, "CdSe nanocrystal quantum-dot memory," *Appl. Phys. Lett.*, vol. 86, 2005, pp. 193106-193109.

[55] A. J. Nozik, "Quantum dot solar cells," *Physica E*, vol.14, 2002, pp. 115-120.

[56] M. T. Harrison, S. V. Kershaw, M. G. Burt, A. L. Rogach, A. Kornowski, A. Eychmüller and H. Weller, "Colloidal nanocrystals for telecommunications. Complete coverage of the low-loss fiber windows by mercury telluride quantum dots," *Pure Appl. Chem.*, vol. 72, 2000, pp. 295–307.

[57] M. Bayer, P. Hawrylak, K. Hinzer, S. Fafard, M. Korkusinski, Z. R. Wasilewski, O. Stern and A. Forchel, "Coupling and Entangling of Quantum States in Quantum Dot Molecules," *Science*, vol. 291, 2001, pp. 451-453.

[58] N. Gaponik, D. V. Talapin, A. L. Rogach, K. Hoppe, E. V. Shevchenko, A. Kornowski, A. Eychmüller and H. Weller, "Thiol-Capping of CdTe Nanocrystals: An Alternative to Organometallic Synthetic Routes," *J. Phys. Chem. B*, vol. 106, 2002, pp. 7177-7185.

[59] A. L. Rogach, T. Franzl, T. A. Klar, J. Feldmann, N. Gaponik, V. Lesnyak, A. Shavel, A. Eychmüller, Y. P. Rakovich and J. F. Donegan, "Aqueous Synthesis of Thiol-Capped CdTe Nanocrystals: State-of-the-Art," *J. Phys. Chem. C,* vol. 111, 2007, pp. 14628-14637.

[60] A. K. Gaigalas and L. Wang, “Measurement of the Fluorescence Quantum Yield Using a Spectrometer With an Integrating Sphere Detector,” *J. Res. Natl. Inst. Stand. Technol.*, vol. 113, 2008, pp. 17-28.

[61] S. Sapra, S. Mayilo, T. A. Klar, A. L. Rogach and J. Feldmann, “Bright White-Light Emission from Semiconductor Nanocrystals: by Chance and by Design,” *Adv. Mater.,* vol. 19, 2007, pp. 569-572.

[62] T. Ozel, I. M. Soganci, S. Nizamoglu, I. O. Huyal, E. Mutlugun, S. Sapra, N. Gaponik, A. Eychmüller and H. V. Demir, "Selective enhancement of surface-state emission and simultaneous quenching of interband transition in white-luminophor CdS nanocrystals using localized plasmon coupling," *New J. of Physics*, vol.10, 2008, 083035-083042.

[63] T. Ozel, S. Nizamoglu, O. Samarska, I. O. Huyal, E. Mutlugun, S. V. Gaponenko and H. V. Demir, "Plasmon Enhanced Colloidal Nanocrystal Composites Incorporating Au Nanoparticles in a Repeating Layered Architecture," *Proceedings of IEEE Photonics* (formerly Lasers and Electro-Optics) *Society 2009 Annual Meeting* (LEOS 2009), Belek-Antalya, Turkey (4 - 8 October 2009). Session: ThD: Quantum Dots, Quantum Wells, and Energy Transfer Paper: ThD 5.

[64] T. Ozel, I. M. Soganci, S. Nizamoglu, I. O. Huyal, E. Mutlugun, S. Sapra, N. Gaponik, A. Eychmüller and H. V. Demir, "Surface-State Emission Enhancement in White-Luminophor CdS Nanocrystals using Localized Plasmon Coupling," *Proceedings of IEEE Lasers and Electro-Optics Society 2008 Annual Meeting* (LEOS 2008), Newport Beach, CA (9 – 13 November 2008). Session: TuQ: Plasmonic. Paper TuQ2.

[65] T. Ozel, S. Nizamoglu, O. Samarskaya, I. O. Huyal, N. Cicek, E. Mutlugun and H. V. Demir, “Plasmon Coupled Förster Resonance Energy Transfer of Quantum Dots,” submitted to *MRS Fall Meeting,* 2009.